Quaternary Science Reviews 177 (2017) 34–56

Contents lists available at ScienceDirect

Quaternary Science Reviews

journal homepage: www.elsevier.com/locate/quascirev

Palaeoenvironments of the last Neanderthals in SW Europe (MIS 3): Cova del Coll Verdaguer (Barcelona, NE of Iberian Peninsula)

J. Daura [a, *], M. Sanz [b, c], E. Allué [d, e], M. Vaquero [d, e], J.M. López-García [d, e], A. Sánchez-Marco [f], R. Domènech [g], J. Martinell [g], J.S. Carrión [h], J.E. Ortiz [i], T. Torres [i], L.J. Arnold [j], A. Benson [k], D.L. Hoffmann [k], A.R. Skinner [l], R. Julià [m]

[a] Grup de Recerca del Quaternari (GRQ)-SERP, Departament d'Història i Arqueologia, Universitat de Barcelona, C/ Montalegre 6, 08001 Barcelona, Spain
[b] Departamento de Paleontología, Facultad de Ciencias Geológicas, Universidad Complutense de Madrid, Ciudad Universitaria s/n, 28040 Madrid, Spain
[c] Centro UCM-ISCIII de Investigación sobre la Evolución y Comportamiento Humanos, Avda. Monforte de Lemos, 5, 28029 Madrid, Spain
[d] IPHES, Institut Català de Paleoecologia Humana i Evolució Social, 43003 Tarragona, Spain
[e] Àrea de Prehistòria, Universitat Rovira i Virgili (URV), Avinguda de Catalunya 35, 43002 Tarragona, Spain
[f] ICP, Institut Català de Paleontologia Miquel Crusafont, Campus de la UAB, 08193 Bellaterra, Spain
[g] IRBio & Departament de Dinàmica de la Terra i de l'Oceà, Facultat de Ciències de la Terra, Universitat de Barcelona.(UB), C/ Martí i Franqués s/n, 08028 Barcelona, Spain
[h] Departamento de Biología Vegetal (Botánica), Universidad de Murcia, 30100 Murcia, Spain
[i] Laboratorio de Estratigrafía Biomolecular, Departamento de Ingeniería Geológica, Escuela Técnica Superior de Ingenieros de Minas, Universidad Politécnica de Madrid C/Rios Rosas 21, 28003 Madrid, Spain
[j] The Environment Institute, Institute for Photonics and Advanced Sensing, School of Physical Sciences, University of Adelaide, 5005 Adelaide, SA, Australia
[k] Max Planck Institute for Evolutionary Anthropology, Department of Human Evolution, Deutscher Platz 6, 04103 Leipzig, Germany
[l] Chemistry Department, Williams College, 47 Lab Campus Drive, 01267 Williamstown, MA, USA
[m] Institut Ciències de la Terra Jaume Almera, CSIC, C/Lluís Solé Sabarís s/n, Barcelona 08028, Spain

ARTICLE INFO

Article history:
Received 3 February 2017
Received in revised form
24 August 2017
Accepted 1 October 2017
Available online 5 November 2017

Keywords:
Late Pleistocene
MIS 3
Cova del Coll Verdaguer
Palaeoenvironment
Iberian Peninsula

ABSTRACT

Marine isotope stage 3 (MIS 3) was characterised by marked oscillations of extreme cold episodes with very short warm events during the stadial, and several regional differences have been recorded in the ice cores and marine deposits. The aim of this study is to reconstruct this period by evaluating both terrestrial and regional responses. Cova del Coll Verdaguer, a site located on the Iberian Peninsula, preserves a sedimentary deposit dated to between 34 and 56 ka BP and provides an opportunity for evaluating the impact of climate changes on the regional landmass during a period that coincided with the last Neanderthal population on the Iberian Peninsula. Several dating methods, including U-series, electron spin resonance, amino acid racemization and radiocarbon (14C), were applied to the site and the ages obtained show good agreement. The biotic evidence obtained is substantial, comprising floristic data from palynology and charcoal analysis, and faunal data from large and small mammals, birds and gastropods. Environmental reconstruction points to an initially open meadow landscape at the base of the sequence (~56 ka) that progressively changes to a woodland environment dominated by conifers (~34 ka). The presence of few thermophilous taxa, in contrast with lower latitudes of the Iberian Peninsula, is also detected. The environmental conditions of mid-altitude, Mediterranean, limestone mountains for the last Neanderthal populations appear to have been dominated by a forested landscape comprising boreal or mixed coniferous forest, characterised by a low usable biomass with poor comestible plant resources and dispersed herbivore populations.

* Corresponding author.
E-mail addresses: jdaura_lujan@ub.edu (J. Daura), msanzborras@ucm.es (M. Sanz), eallue@iphes.cat (E. Allué), manuel.vaquero@urv.cat (M. Vaquero), jmlopez@iphes.cat (J.M. López-García), antonio.sanchez@icp.cat (A. Sánchez-Marco), rosa.domenech@ub.edu (R. Domènech), jmartinell@ub.edu (J. Martinell), carrion@um.es (J.S. Carrión), joseeugenio.ortiz@upm.es (J.E. Ortiz), trinidad.torres@upm.es (T. Torres), lee.arnold@adelaide.edu.au (L.J. Arnold), alexa_benson@eva.mpg.de (A. Benson), dirk_hoffmann@eva.mpg.de (D.L. Hoffmann), askinner@williams.edu (A.R. Skinner), nomar.ailuj@gmail.com (R. Julià).

https://doi.org/10.1016/j.quascirev.2017.10.005
0277-3791/

1. Introduction

Climate conditions during Marine Isotope Stage 3 (MIS 3) (ca. 57–29 ka) have been widely reported on the basis of marine deposit and ice-core records (Cacho et al., 1999; Lisiecki and Raymo, 2005; Sanchez Goñi and Harrison, 2010), pointing to the extreme variability of this period. For example, high-resolution analyses of marine sediment were used to reconstruct MIS 3 conditions on the basis of palynological data (Fletcher and Sánchez Goñi, 2008) and sea-surface temperatures, among others (Martrat, 2004). The vegetation and fauna records reflect the alternation between relatively forested and more open landscapes, which parallels oscillating periods of abrupt warming and cooling documented in marine cores, i.e. Heinrich Events or Dansgaard-Oeschger (D-O) oscillations, respectively (Fletcher et al., 2010).

Evidence of the climate and environment during MIS 3, as derived from terrestrial archives, is typically imprecise and fragmentary because long stratigraphic sequences are rare. Several simulation models have been developed to reconstruct the terrestrial response to climate oscillations (Sánchez Goñi et al., 2002; Sepulchre et al., 2007). Another approach involves conducting archaeological and paleontological studies in caves and rock-shelter sites (Burjachs et al., 2012; Jennings et al., 2009; López-García et al., 2010) to obtain more direct evidence, while speleothems have been used to reconstruct temperature changes during this period in the Mediterranean Basin and SW Europe (Bar-Matthews et al., 2003; Hodge et al., 2008; Wainer et al., 2011).

The archaeological evidence indicates that at MIS 3 – primarily during Heinrich Event 4 (HE 4) – the arrival of early modern humans and the disappearance of Neanderthals in the Iberian Peninsula occurred. This is one of the most critical events in human evolution in the European realm, especially in the Iberian Peninsula where the Neanderthals seem to have survived longer than elsewhere in SW of Europe (Finlayson et al., 2006; Zilhão, 2009). The possible impact of the MIS 3 climate oscillations and the extreme aridity of HE 4 on Neanderthal extinction has long been the subject of intense debate. Indeed, palaeoenvironmental studies highlight the significant climate fluctuations occurring during this period, which seem likely to have played a role in this event and in the late dispersal of early modern Europeans (Carrión, 2004; d'Errico and Sánchez Goñi, 2003; Finlayson, 2004; Sepulchre et al., 2007). Floristic data suggest landscapes of patched vegetation cover during the Late Pleistocene in the Iberian Peninsula and a marked gradient between northern and southern latitudes (Finlayson and Carrión, 2007; González-Sampériz et al., 2010).

Unfortunately, the period when the last Neanderthals inhabited SW of Europe (MIS 3) lies beyond the limits of radiocarbon dating. Besides, chronological analyses of related sites are typically based on questionable ages provided by samples contaminated with residual radiocarbon. Indeed, recent studies demonstrate the problem of undertaking reliable decontamination of samples and conclude that the ages obtained may be younger than actual ages (Higham et al., 2009; Maroto et al., 2012; Talamo et al., 2016; Wood et al., 2014, 2013). As a result, many archaeological sites chronologically placed near the time limit of the radiocarbon method (~post-45 ka cal BP) and, therefore, with an unreliable chronology, are used to reconstruct the palaeoenvironmental conditions of the MIS 3.

To counter these shortcomings, this work aims to define the palaeoecological conditions of the last Neanderthal population in the Iberian Peninsula from ca. 34 to 56 ka. The charcoal, pollen, large and small mammals, bird and snail records of the archaeological site of Cova del Coll Verdaguer are analysed and supported by the combination of 27 datings by means of U-Th, radiocarbon, electron spin resonance, thermoluminiscence, and amino acid racemization techniques. The multi-proxy information from this site provides a clearer picture of the impact of climate fluctuations that coincide with the extinction of the last Neanderthal population in the west of the Mediterranean Basin.

2. General setting and site description

Cova del Coll Verdaguer (coordinates: 41°23′35.08″N, 1°54′39.81″E 448 m a.s.l.) is located in the northern Garraf Massif, at the top of hill known as Coll Verdaguer (Cervelló), 30 km to the southwest of Barcelona (NE of the Iberian Peninsula) (Fig. 1.1 and 1.2). The cave is located at a distance of 15 km from the current sea shore and the drainage basin of the region is limited now to the Sant Ponç dry valley tributary of the Rafamans creek. Today, the region occupies the meso- and thermo-Mediterranean environments, composed mainly of the Mediterranean maquis shrubland, with a high density of evergreen shrubs, and forests with sclerophyll vegetation that can endure the dry season. Modern climate data (last 30 years) from the meteorological station at Barcelona Airport, located at 6 m a.s.l and about 15 km to the south-west of the site, show a mean annual temperature (MAT) of 15.6 °C and a mean annual precipitation (MAP) of 659 mm (Font-Tullot, 2000).

The massif constitutes a low relief, intensely karstified, mountain range that rises to a height of close to 600 m. A simple five-stage geomorphological model of the evolution of the Garraf karstification has been proposed between the Miocene and the Holocene (Daura et al., 2014). The karstification of the Garraf massif is highly local and concentrated in the fractured carbonate rocks. The main karst features include dolines, shafts and caves (Daura et al., 2014). From a geological point of view, the limestone massif is affected by an antiform (Bartrina et al., 1992), and a series of fractures trending predominantly NE to SW run across the entire massif (Guimerà, 1988). The cave, formed in brecciated dolostones of the basal Cretaceous, was partially destroyed during the first-half of the 20th century by mining for sparry calcite (Bogatell, 1930).

Cova del Coll Verdaguer is a karst cave and was first visited in 1936 by Llopis Lladó (1941). During the 1960s, archaeological remains were identified and the site was excavated by amateur archaeologists from the *Centre Excursionista de Vallirana*, although their results were not published. It was not until the 1990s and a geological expedition conducted by J. M. Cervelló that the cave's potential as an archaeological site was made known. Current archaeological research was initiated in 2004 by the *Grup de Recerca del Quaternari* (GRQ), which has been responsible for describing its sedimentological framework (Daura, 2008) and the faunal and coprolite assemblage (Sanz, 2013).

The original cave entrance was completely sealed by a cemented collapse deposit (Fig. 1.3 and 1.5), but it was carved during current archaeological fieldwork (Fig. 1.4 and 1.6). However, the cave could be accessed through two other artificial entrances (named Rampa and Shaft), which were partially excavated when the cave was being mined for sparry calcite. The cave consists of an artificial chamber named Sala dels Miners (15 × 10 m) excavated during mineral extraction, although this chamber was later partially filled by rubble composed of a mixture of Pleistocene sediments and mine deposits, and two other chambers filled with Late Pleistocene sediments. Sala Sal de Llop (7 × 5 m) is the chamber located closest to the cave entrance, and after being carved is now partially exposed to daylight, while Sala dels Ursus (10 × 10 m) is located in the inner part of the cave, at a lower altitude and filled with displaced sediments from Sala Sal de Llop.

3. Materials and methods

3.1. Excavation methodology

Archaeological work to date has focused on excavating and

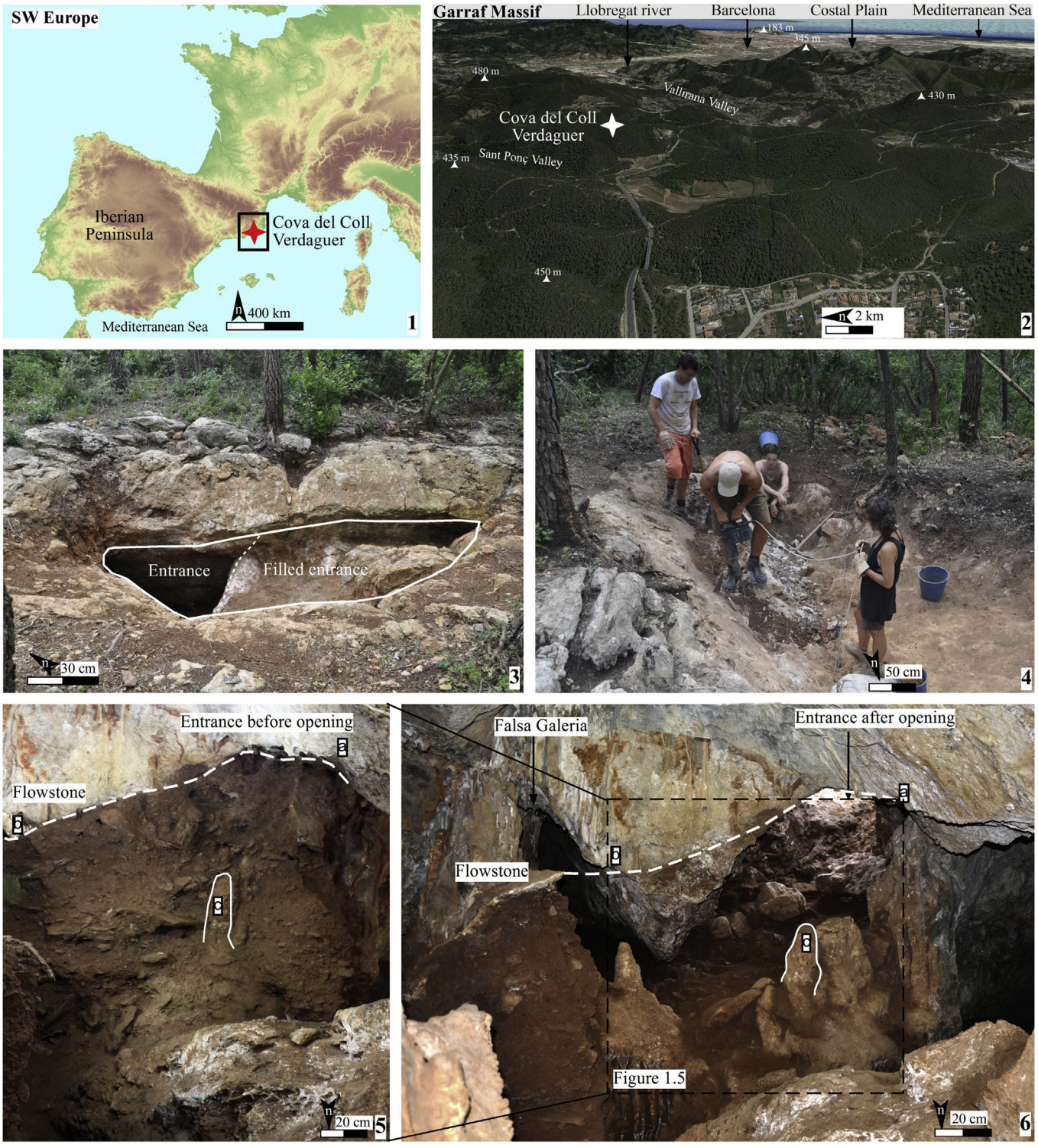

Fig. 1. Cova del Coll Verdaguer. 1: Location of the archaeological site. 2: View of cave entrance. 3: Site plan showing distinct areas of cave and speleogenetic phases. 4: Filled entrance during reopening. 5. Original filled entrance before reopening the cavity. 6: Entrance after removing debris that filled the original entrance (Correlation with Fig. 1.5 and 1.6 is indicated by letters a, b, and c).

sampling the area closest to the original entrance (Sala Sal de Llop) and on sampling speleothems in other areas (Sala dels Ursus). In addition, the rubble accumulated as a result of mining activity has been sieved; however, these recovered materials are not reported here as their exact stratigraphic provenience is not easily constrained.

Excavation work has been carried out using standard archaeological and palaeontological techniques, with three-dimensional plotting of finds. Blocks and cobbles c. 15 cm in diameter, stone tools, large mammal bones, lagomorph cranial remains and charcoal fragments were mapped *in situ* prior to removal, while land snail shells and lagomorph post-crania were bagged by 1-m^2 units

of provenience. Sediments were dry sieved using superimposed 5- and 1-mm mesh screens. Recovery of micromammal remains and other small bones was carried out by the wet sieving of the 2.0- to 0.4-mm fraction in our archaeological laboratory.

Excavation of the sediments was performed with fine tools because the sediment was soft, except in the entrance area and in specific areas inside the cave where the sediment was highly cemented. The palaeontological remains were partially encased in calcareous breccias that had to be restored using normal air scribe (Mod. W 224), and consolidated with Paraloïd-B72 dissolved with acetone.

The burrow trails of fossorial animals were observed at the time of excavation in the three units. The sediment contained in these burrows was excavated separately from each unit to avoid bioturbated elements. The material contained inside the burrows is not included in the present study.

The site was excavated according to the identified geological stratigraphy of the infill. Layers were grouped in three main units numbered from the top of the stratigraphic sequence.

3.2. Sampling and laboratory methods

Five dating methods were used to establish a chronological framework for the site. U-Th dating of the flowstone that caps the deposit and the speleothems formed above the bedrock and buried by the deposit provides minimum and maximum ages for the accumulation. Radiocarbon dating was used to constrain the chronology of the upper part of the sequence, while complementary dating methods, including TL, ESR and AAR, were used to evaluate the integrity of the deposit. Samples were selected from the three main units identified at the site and their stratigraphic provenience is shown in Fig. 3. Palaeoenvironmental reconstruction was based on multi-proxy analyses: vegetation remains were determined from pollen analyses of hyena coprolites and from charcoal fragments; faunal remains were analysed in the bone and teeth remains of small and large mammals and birds, and malacology was studied in shell fragments.

3.2.1. U-series dating of speleothems

In cave environments, water-soluble uranium isotopes co-precipitate at the time of calcite deposition, but insoluble daughter isotopes (like Th isotopes) are initially not present leading to an initial U-Th disequilibrium (Ivanovich and Harmon, 1992).

After the calcite formed, the activity of the daughter isotopes of the uranium decay chain starts to grow back to equilibrium and todays activity ratios can be used to calculate the time since formation, i.e. the age of the calcite. The clock stops once activity equilibrium is reached. However, the dating method can only be reliably applied if (a) the material (calcite) is and always was a so-called closed system, i.e. neither U nor Th were added or removed at any time after formation, and (b) no Th was co-precipitated, i.e. no initial presence of Th in the calcite.

Initial presence of Th is often found where detrital particles, e.g. clay, are incorporated in the calcite. However, detrital components also harbour large amounts of ^{232}Th ('common' thorium), which is not part of the ^{238}U-^{234}U decay series; hence, the presence of ^{232}Th serves as an indicator for detritus and the ^{230}Th/^{232}Th activity ratio is used to assess the degree of contamination (Bischoff et al., 1988). A correction is then made using a measured or assumed value for the detrital ^{238}U/^{232}Th activity ratio.

For this study, a total of seven carbonate samples were dated using the U-Th disequilibrium method. One of the samples (#4) was collected from the inner chamber (Sala dels Ursus), while the other six samples (#1, #2 #3, #5, #6 and #7) were taken from different areas of the excavation zone (Sala Sal de Llop). The analyses were done in two different laboratories, one using alpha spectrometry, and one using MC-ICPMS techniques.

3.2.1.1. MC-ICPMS U-series dating of speleothems. Sample preparation and purification follows procedures detailed in Hoffmann et al. (2016). In short, samples are weighed and then MilliQ (MQ) water is added. The sample is then dissolved by adding sufficient 7 M HNO_3 to completely dissolve the. A mixed ^{229}Th-^{236}U tracer is then added to the solution. The solution on a hotplate to equilibrate sample and spike and then evaporated to dryness. The sample is dissolved in 50 μl concentrated HNO_3 plus 50 μl concentrated $H_2O_2$and the solution heated at 90 °C for several hours. Then, 50 μl concentrated HCl is added to the solution, placed again on a hotplate at 90 °C for a minimum of 12 h and finally dried down. The sample is dissolved in 6 M HCl for separation and purification chemistry, which consists of a double resin procedure with AG 1 × 8 used to separate U and Th followed by a first Th fraction purification using AG 1 × 8. Final purification of U and Th fractions is done using UTEVA resin. U and Th isotope compositions are measured by MC-ICPMS using a ThermoFinnigan Neptune and a CETAC Aridus II, following procedures outlined in Hoffmann et al. (2007). The following decay constants are used to calculate activity ratios: $\lambda_{238} = (1.55125 \pm 0.0017)\cdot 10^{-10}$ a^{-1} (Jaffey et al., 1971) $\lambda_{234} = (2.826 \pm 0.0056)\cdot 10^{-6}$ (Cheng et al., 2000), $\lambda_{232} = (4.95 \pm 0.035)\cdot 10^{-11}$ (Holden, 1990), $\lambda_{230} = (9.1577 \pm 0.028)\cdot 10^{-6}$ (Cheng et al., 2000).

3.2.1.2. Alpha spectrometric U-series dating of speleothems. U-Th dating of speleothem samples #2, #3, #4 and #6 was done using alpha spectrometric methods at the Institut de Ciències de la Terra "Jaume Almera" (Barcelona). Numerical ages are calculated directly from the daughter/parent activity ratio of ^{230}Th/^{234}U, assuming that all the measured ^{230}Th was formed by *in situ* decay of the ^{234}U and ^{238}U originally present. The procedure used for chemical separation and purification was conducted in line with Bischoff and Fitzpatrick (1991): samples were totally dissolved in mineral acids and an artificial radioisotope with known activity was incorporated into the solution to determine the efficiency of the isotope separation. The U and Th isotopes were isolated by ion-exchange chromatography and then analysed by an alpha spectrometer from Ortec Octete Plus with a silica barrier detector. Rosenbauer (1991) UDATE program was used for age calculation.

3.2.2. Radiocarbon dating

Given the absence of collagen in the archaeological bones, three pieces of *Pinus sylvestris* type charcoal were selected (samples #8 and #9 from Unit 1 and sample #10 from Unit 2). The samples (#8, #9, #10) were selected for dating with an accelerator mass spectrometer (AMS) at the Radiocarbon Accelerator at Oxford University and calibrated using the IntCal 13 curve (Reimer, 2013) and OxCal v4.2 software (Bronk Ramsey, 2009). The samples correspond to charcoal fragments (*Pinus* t. *sylvestris* type) from Units 1 and 2 and they were pre-treated using the ZR protocol (Brock et al., 2010).

3.2.3. Electron spin resonance (ESR) dating

Electron spin resonance (ESR) dating is part of the family of 'trapped charge' geochronology methods. Details of the method can be found in Rink (1997) and Skinner (2014). Eight tooth and bone samples were selected for ESR dating in the present study (#12, #14, #16, #17, #18, #20, #21, #22) but only three (#12, #21 and #22) proved successful: two specimens from Unit 3 and one from Unit 2. As the hardest substance in the body, tooth enamel is often well preserved in archaeological and paleontological sites, and the ESR signal lifetime exceeds several million years (Schwarcz, 1985;

Skinner et al., 2000). It therefore represents a dating material for constraining the age of faunal remains at sites such as Cova del Coll Verdaguer. Tooth samples were prepared by standard methods (Blackwell et al., 2016) and were artificially irradiated with a ^{60}Co source (~2 Gy/min) for palaeodose (A_Σ) determination. ESR spectra were measured on a JEOL RE1X spectrometer, using a field centre at 340 mT, power of 2 mW, modulation amplitude of 01 mT, and scan speed of 1.25 mT/min. The ESR dose-response curve was constructed from at least 12 different doses and the corresponding A_Σ was calculated using VFit. Radioisotope contents in the tooth and surrounding sediment were determined by neutron activation analysis (NAA) and converted to internal and external dose rate estimates. The final ESR ages were calculated using the Data-HPS program.

An important consideration in ESR dating studies is post-depositional absorption of U by teeth, which has an effect on the internal dose rate calculation. Traditionally, this complication has led to routine reporting of three possible ESR ages, each related to different assumptions about U uptake history: the Early Uptake (EU) model assumes that all U was absorbed shortly after burial and yields the youngest age; the Linear Uptake (LU) model assumes continuous uptake during burial; and the Recent Uptake (RU) model assumes that a change in the sample environment shortly before excavation led to most of the U uptake occurring late in the burial history. RU models therefore yield the oldest ESR ages for a given sample. Coupled U-series/ESR dating has allowed more reliable age determinations from different models of U uptake history (Grün and McDermott, 1994). However, the tooth fragments found at Cova del Coll Verdaguer were small and did not contain enough U to allow for coupled U-series/ESR dating. Consequently, the ESR ages are reported as model-dependent estimates. LU ages are generally assumed to be reliable on the basis of independent dating comparisons; indeed, in sites where cross-calibration has been possible between two (or more) dating methods, the LU model typically yields the closest age agreements (Porat and Schwarcz, 1994). However, this outcome cannot be guaranteed for all samples and sedimentary contexts. Sites with reliable RU ages are rare, but not unknown (Blackwell et al., 2007).

Environmental factors that may affect the trapped charge method and which may change over time include the water content of the sediment, sediment inhomogeneity, radon mobility, and the cosmic radiation if the cover changes. Cave environments are more stable than the open air and, hence, the only environmental factor likely to change significantly is water content, which may well have been exposed to wet/dry cycles and, moreover, the position of the modern water content in this cycle cannot be determined absolutely. Fig. 4 seeks to show how this uncertainty might affect the ages quoted. An increase in water content would reduce the external dose rate and increase the age, whereas a decrease in water content would, logically, reduce the age. The endpoints of Fig. 4 represent, in the first place, a water content of 40% and an age of 52 ka, and, second, a water content of 10% and an age of just under 43 ka. Within the 1σ uncertainty, the percentage of water does not affect the age.

3.2.4. Thermoluminescence (TL) dating

TL dating was used to constrain the depositional age of unheated sediments from Unit 2 (sample #11) of Cova del Coll Verdaguer, assuming solar resetting of the luminescence signal to a low and measurable residual level prior to burial. A single sediment sample was collected from a cleaned exposure of Unit 2 under strictly controlled lighting conditions at the Laboratorio de Datación y Radioquímica, Universidad Autónoma de Madrid (Spain).

The TL signals of the prepared silicate fractions (2–10 μm) were measured using a Risø TL-DA-10 reader equipped with a calibrated ^{90}Sr/^{90}Y beta source. Ultraviolet TL emissions were detected using an EMI 9235QA photomultiplier tube fitted with a 7.5-mm-thick Hoya U-340 glass filter. Equivalent dose (D_e) values were determined using a 'total bleach' multiple-aliquot additive dose (MAAD) protocol (Aitken, 1985), which involved a preheat of 90 °C for 120 s and subtraction of a laboratory determined residual that was presumed to be similar to any remnant (hard-to-bleach) TL signal remaining in nature. TL plateau tests were used to isolate the thermally stable and easy-to-bleach region of the TL glow curve for the MAAD protocol. These corresponded to the 300–350 °C region of the TL glow curve for sample #11. Separate groups of undosed (natural) and laboratory dosed (natural + dosed) aliquots containing several thousand grains were measured as part of the MAAD protocol ($n = 4$ aliquots per group). Ten replicate D_e estimates were measured for the sample and used to calculate a mean burial dose estimate for the final age calculation.

The environmental dose rate of the sample was determined using a combination of low-level beta counting and thick-source alpha counting. Cosmic-ray dose rate contributions were calculated from high energy gamma emissions recorded *in situ* using a NaI(TL) gamma spectrometer. Alpha dose rates were calculated using an empirically determined alpha effectiveness (*a*-value) of 0.17, which was calculated by comparing the TL signals induced by 3.7 MeV alpha particles (using a ^{241}Am source) with corresponding TL signals induced by beta irradiation (using the ^{90}Sr/^{90}Y source) for the sample (Zimmerman, 1971). The final dose rates were also adjusted for water attenuation effects (Aitken, 1985), using present-day sediment moisture contents.

3.2.5. AAR dating of shell fragments

Peripheral parts of the gastropod shells (approximately 20–30%) of the family Helicidae were removed after chemical etching with 2 N HCl. They were carefully cleaned by sonication in distilled deionized (DDI) water and rinsed with DDI water to remove sediment.

The amino acid epimerization/racemization analyses of four samples (#25, #26, #27 and #28) were performed in the Biomolecular Stratigraphy Laboratory (Madrid, Spain). Amino acid concentrations and D/L values were quantified by high performance liquid chromatography (HPLC) following the sample preparation protocol described by Kaufman and Manley (1998) and Kaufman (2000). Samples were injected into an Agilent-1100 HPLC equipped with a fluorescence detector. Excitation and emission wavelengths were programmed at 335 nm and 445 nm, respectively. A Hypersil BDS C18 reverse-phase column (5 μm; 250 × 4 mm i.d.) was used for the separation.

Ages were estimated using the age calculation algorithms established by Torres et al. (1997) for the central part of the Iberian Peninsula. The use of these algorithms for the dating is applied of these deposits is justified on the grounds that a similar thermal history can be inferred for this area and for Coll Verdaguer, located in the Mediterranean-pluviseasonal climatic zone of the Iberian Peninsula, and Italy, respectively, with a similar CMAT (Rivas-Martinez and Rivas-Saenz, 1996–2017).

3.2.6. Palaeobotanical analyses

Floristic analyses were conducted on charcoal fragments and pollen from ten coprolites. All the coprolites belonged to Morphotype 1 described by Sanz et al. (2016), and were characterised by their globular or spherical morphology and ascribed to hyena. In the laboratory, the coprolites were cut open with a steel spatula, and material from the centre was scraped out to minimize contamination from external surfaces, and weighed. Laboratory treatment was performed following conventional HF, HCl, KOH/NaOH methods and *Lycopodium clavatum* tablets containing a

known quantity of spores were added to each sample to calculate the pollen concentration. Pollen grains were concentrated by means of Thoulet's heavy-liquid flotation. The pollen diagram was constructed using *p*-simpoll software (Bennett, 2000). Percentages of each taxon in each sample were based on a pollen sum (c. 150–2000 grains) excluding hydro-hygrophytes and non-pollen microfossils.

Charcoal analyses were carried out on 755 remains previously collected by hand and by the bucket flotation of sediment samples. Most of the charcoal samples were recovered from Units 1 and 2, whereas Unit 3 provided just 26 remains. Identification of charcoal was carried out using the standard anthracological method (Chabal et al., 1999). Each charcoal fragment was hand-fractured in order to obtain the three anatomical sections and so permit examination of their wood cell structure. Observations were carried out using the optical microscope Olympus (BX41).

3.2.7. Palaeontology

To reconstruct the palaeoenvironmental conditions of the archaeological site, several groups of animals were anatomically and taxonomically classified using classic palaeontological methods. The materials were identified using the skeletal reference collections available at each host institution and following the general criteria provided by the literature for each group, as follows: Furió (2007) and López García et al. (2015) for insectivores and rodents; Lister (1996) for cervids; Crégut-Bonnoure (2005) for caprids; Fick (1974) and Sánchez-Marco (1996) for birds; and Adam (1960), Borredà et al. (2010), Cadevall and Orozco (2016) and Welter-Schultes (2012) for malacological specimens.

For vertebrates (large mammals, micromammals and birds), taxonomic assignments, a Minimum Number of Individuals (MNI) index and a Number of Identified Specimens (NISP) for each taxon were established following standard zooarchaeological methods (Reitz and Wing, 2008; Stiner, 2005). The analysis of leporids is not included here; however, the MNI and the NISP counts were estimated based on mandibles. Invertebrate remains (gastropods) were also identified and the MNI index was estimated.

4. Results

4.1. Speleogenesis and stratigraphy

Two lengthwise (Fig. 2.3 and 2.4) and one widthwise (~15 m) (Fig. 2.2) stratigraphic cross-sections and one column (Fig. 3.1) can be drawn in order to describe the lithological succession at the site of Cova del Coll Verdaguer. The lithostratigraphic units can be defined by their geological features and five main stratigraphic units have been recognized: Large Block Unit (LBU), Lower Speleothem Unit (LSU), Debris Cone Unit (DCU), Upper Flowstone Unit (UFU) and Sal de Llop Mining Unit (SMU).

The lowermost unit exposed to date at the cross-sections is the Large Block Unit (LBU), corresponding to very large (~2–5 m) parallelepipedic blocks without any matrix. The unit probably collapsed from the ceiling, the result of two fractures oriented NE-SW and NW-SE, respectively. The maximum exposed thickness is about ~2 m; however, the bedrock has not been reached and no archaeological or palaeontological remains have been recovered.

The Lower Speleothem Unit (LSU) is the second unit to have developed on top of these large blocks (LBU). It corresponds to well-developed speleothem formations, composed of flowstones and stalagmite formations. The speleothem formation is of variable texture, crystallinity and thickness (between 5 cm and 1 m), depending on local factors and the cave environment.

Another distinct facies is recognized above the LSU unit. The LSU unit is covered by a debris cone (DCU), which filled up the main chamber (Sala Sal de Llop) and sealed the cave. The stratigraphic thickness of this cone deposit is irregular and accommodates large blocks (LBU) and speleothems (LSU) (Fig. 2.1 and 2.2). The 3.5-m sequence of the DCU unit in the middle of the Sala Sal de Llop chamber (square H8) decreases in thickness to 1.2 m at the entrance and 0.4 m at the back of the chamber (Fig. 2.3 and 2.4). This is where most of the remains contained in Units 1, 2 and 3 derive from.

The uppermost Late Pleistocene unit corresponds to a new, well-developed speleothem formation (Upper Flowstone Unit: UFU) developed on top of the sediments and which seals the entire deposit. This unit consists chiefly of a characteristic cave flowstone, which presents different degrees of crystallinity and purity with a thickness of between 2 and 10 cm. Several bones were partially covered by this formation. However, mining resulted in an erosive process that emptied the uppermost units and filled the gallery (Sala dels Miners) with rubble, which accumulated as a direct result of quarrying (Sal de Llop Mining Unit: SMU).

Archaeological excavations at Cova del Coll Verdaguer have focused above all on the DCU unit, which corresponds to the package of sediments containing the archaeological and paleontological materials. For this reason, we describe this unit in detail below.

DCU sediment is very similar in grain size, number and size of clasts and colour. Many lateral and longitudinal discontinuities were recognized during the excavation based on the cone deposition; however, it has been grouped in three main units (Fig. 3.1). The cave sediments are composed chiefly of rock fragments (dolostone and speleothem) in a clast- or matrix-supported fabric and the archaeological excavation revealed a preferential orientation of NW-SE and a dip of about 18–25°. The large-sized blocks probably accumulated from the cave walls and the roof and the smaller size components of the breccia may be derived from the cave entrance accumulated by occasional rainfall-triggered, debris flow events.

Unit 1 is the uppermost unit sealed by the uppermost flowstone (UFU) (Fig. 3.2 and 3.3) and extends from 0 to −90 cm below datum. This unit located in the cave entrance and in Sala Sal de Llop is formed by angular clasts of 25–35 cm in size, with a fine matrix. This unit alternates several chaotic phases of block accumulation (25–35 cm) filled with fine sediment. Several fine horizons of charcoal accumulations have also been detected but no evidence of combustion structures or burnt sediment has been documented during the excavation. Based on the cave morphology and Unit 1 topography, access to the cave was, at the time of its formation, highly restricted (>~1 m of diameter).

Unit 2 is the middle unit and develops from −100 cm to −140 cm below datum. We did not identify this unit at the back of the gallery, where the excavation reached the LBU unit, or at the entrance, where the excavation did not reach the base. The reduced thickness, the high degree of block accumulation and the reduction in the matrix result in a lower presence of archaeological and paleontological materials which, nevertheless, tend to accumulate at the base (Fig. 3.6). The top of this unit is mainly composed of blocks (20 cm in size), while at the base the matrix component is more abundant. Charcoal accumulation and small pieces of burnt sediment have been documented corresponding probably to a fireplace (EC1) (Fig. 3.4 and 3.5).

Unit 3 corresponds to the lowermost unit lying on the LBU and LFU units. It is only located in the central part of the Sala Sal de Llop where the uniformities of the large blocks created a deep depression. This unit is a very humid and soft mud-supported breccia. The bone concentration is greater in this unit than it is in Units 1 and 2.

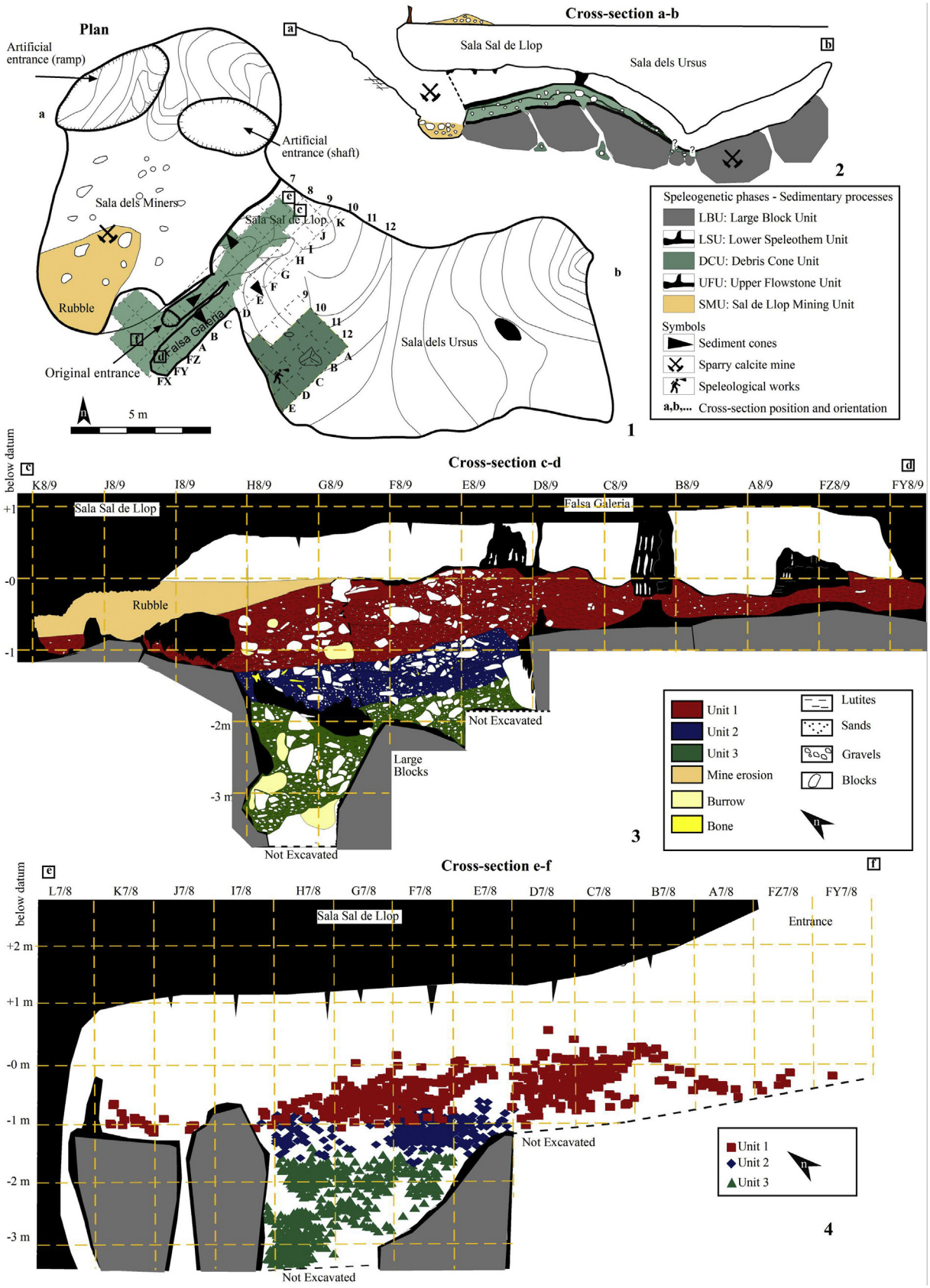

Fig. 2. Cave formation and sedimentary processes. 1: Plan site of Cova del Coll Verdaguer showing the different parts of the archaeological site. 2: W-E cross-section of the cavity showing the main speleogenetic phases. 3: N-S cross-section showing three main stratigraphic units. 4: N-S cross-section with archaeological artefacts plotted and grouped according to distribution in three main units (the position and orientation of the cross-sections are marked in the plan site using letters a-b, c-d and e-f).

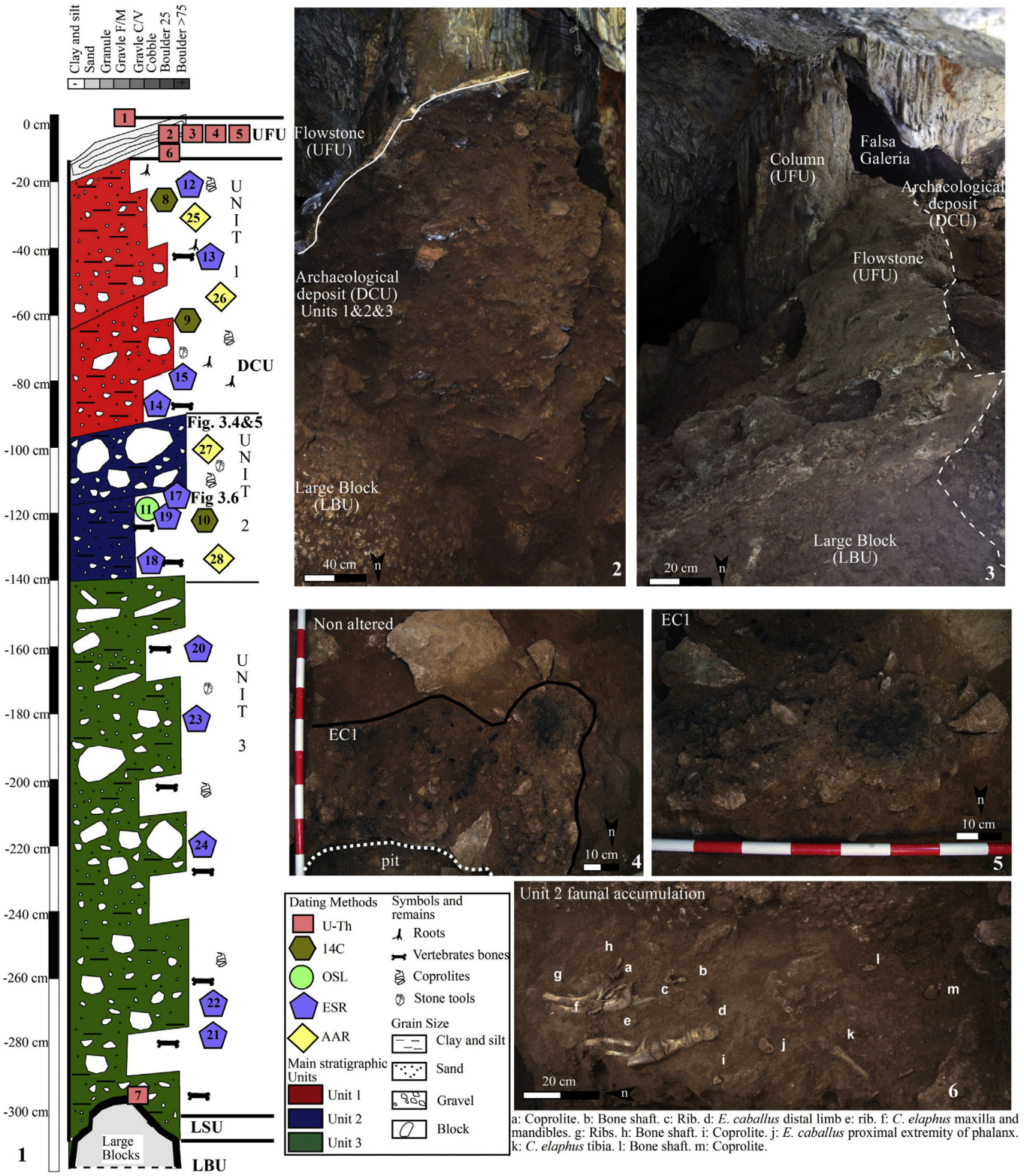

a: Coprolite. b: Bone shaft. c: Rib. d: *E. caballus* distal limb e: rib. f: *C. elaphus* maxilla and mandibles. g: Ribs. h: Bone shaft. i: Coprolite. j: *E. caballus* proximal extremity of phalanx. k: *C. elaphus* tibia. l: Bone shaft. m: Coprolite.

Fig. 3. Stratigraphy and sampling. 1: Stratigraphic column of Cova del Coll Verdaguer showing the position of the U-Th, 14C, TL, ESR, and AAR samples. 2: Main stratigraphic Units 1 and 2. 3: Flowstone located at the top of Unit 1. 4: Charcoal accumulation EC1 from the horizontal view. 5. EC1 in 45° view. 6: Unit 2 faunal accumulation.

4.2. Dating evidence

4.2.1. U-Th dating

U concentrations derived for four samples by alpha spectrometry are highly variable between 0.01 and 1.124 μg/g. U concentrations of the three samples analysed by MC-ICPMS methods are all between 0.21 and 0.25 μg/g. There are significant levels of common thorium for most samples, with 230Th/232Th

activity ratio smaller than 12. For these samples a detrital correction is significant. For one sample, measurement of 232Th failed. Only one sample (#5) has a small and negligible detrital component with 230Th/232Th > 200. Analytical results and corresponding U-Th ages are presented in Tables 1 and 2.

Four of the samples (#2 to #5) correspond to the lowermost horizontal layers of a flowstone formation. The U-Th ages show some scatter with 19.3 ± 0.7, 17 ± 0.4, 15.9 ± 0.7 and 14.4 ± 0.2 ka, respectively. Three alpha spectrometric results indicate that the flowstone formed during GS-2 (Rasmussen et al., 2008). The more precise MC-ICPMS on a sample with no significant detrital correction yields an age that falls into the Bolling/Allerod. Sample (#1), corresponding to the uppermost flowstone layer, yields an age of 5.0 ± 2.9 ka and falls into the Holocene.

Sample #6 yielded an age of 38.3 + 2.3/-2.2 ka and corresponds to carbonates formed at the base of the flowstone. The U-Th ages of the capping flowstone post-date that of the cave infill, indicating that no sedimentation occurred in the cave during this period (38–5 ka), a period of mostly arid conditions as indicated by the lakes and speleothems in the Iberian Peninsula (Moreno et al., 2010; Stoll et al., 2013). However, others scholars show enhanced precipitation in Spain between 29 and 25 ka (Domínguez-Villar et al., 2013; Hoffmann et al., 2017).

Sample #7 corresponds to a stalagmite of the LSU formed on top of LBU and was fully covered by archaeological infill (DCU). The age of 90.4 ± 4.0 ka pre-dates that of the entire deposit, i.e. it represents a maximum age for the sediment accumulation.

4.2.2. Radiocarbon dating

The radiocarbon dating results obtained for Cova del Coll Verdaguer are shown in Table 3. The ages reported are statistically indistinguishable at 2σ confidence. Sample (#8), sited at the top of the sequence, presents the most recent radiocarbon age and is, according to the U-Th dating (section 4.2.1) of the capping flowstone. Sample (#9) appears to be older than sample (#8), in terms of their respective 2σ calibration ages, but the sample from Unit 2 (#10) seems to be slightly younger than this intermediate sample; however, when considering their 2σ uncertainty ranges, it could be older. The radiocarbon ages indicate that the reference age range of Unit 1 is 41–45 ka cal BP and that the age range of Unit 2 is 42–43 ka cal BP. However, it cannot be ruled out that the radiocarbon ages are minimum age estimates, as they are at the limit of the ^{14}C dating technique.

4.2.3. TL dating

Sample #11 provided an average MAAD D_e value of 121 ± 8 Gy and a total dose rate of 2.61 ± 0.15 Gy/ka (Table 4). These TL results yield an age of 46.6 ± 4.2 ka (1σ uncertainty range) for the middle of Unit 2, which suggests that the lower part of this unit was deposited during MIS 3. In assessing the reliability of this TL age, it is worth considering two potential complications in further detail. First, we run the risk that the multiple-grain aliquot D_e values have been derived from sub-populations of insufficiently bleached grains (Arnold and Roberts, 2011, 2009; Arnold et al., 2011, 2009, 2007), this would cause a systematic overestimation of the true burial age because the residual TL levels determined in the laboratory as part of the 'total bleach' protocol would not be representative of the residual levels experienced by the grain populations measured in nature. Second, we face the likelihood that the TL signals measured are in part derived from potassium feldspar grains, which are known to suffer from age underestimation related to long-term signal instability (so-called anomalous fading) (Huntley and Lamothe, 2001; Wintle, 1973).

The presence of insufficiently bleached grain populations is a possible concern given the sedimentological context of the site (i.e. a karst cave setting with limited potential for daylight exposure during alluvial infilling), and the scale of the D_e measurements adopted in this study (multiple-aliquot; several thousand grains per aliquot). However, seemingly reliable total bleach MAAD TL ages have been reported for similar cave settings located elsewhere in Spain (Berger et al., 2008; Daura et al., 2015). Additionally, the TL signal used here for MAAD D_e determination was derived primarily from the 'rapidly bleaching' 325 °C TL peak, which corresponds to the main source trap used for optically stimulated luminescence (OSL) dating (Spooner, 1994). By targeting the 300–350 °C region of the TL glow curve, it is likely that contributions from more problematic 'slowly bleaching' TL peaks (particularly the 375 °C TL peak) have been minimised or largely avoided in this study.

Multiple aliquot storage tests conducted on sample #11 at the Laboratorio de Datación y Radioquímica (Universidad Autónoma de Madrid) suggest that the targeted TL signal may not be significantly affected by anomalous fading – signal losses were reported to be within analytical uncertainties (<3%) following storage times of 240 h. The lack of significant signal loss following laboratory storage may reflect the absence, or near absence of feldspar grains in the silicate-rich fine-grained fractions of the sample. However, the inclusion of a small number of feldspar grains seems likely when using standard TL preparation procedures and any minor populations of feldspar grains may still be sufficient to dominate the measured TL signals given their intrinsically bright luminescence intensities. Anomalous fading of polymineral TL has been shown to be a near ubiquitous problem across a wide range of geological provinces (Aitken, 1998, 1985; Huntley and Lamothe, 2001; Wintle, 1973). It therefore seems plausible that the low levels of signal loss recorded for this sample reflect the practical difficulties of obtaining reliable and precise fading assessments using non-normalised MAAD procedures (Aitken, 1998). More rigorous, sensitivity-corrected single-aliquot regenerative-dose anomalous fading tests were not performed on these samples following the widely adopted procedures of Auclair et al. (2003) and Huntley and Lamothe (2001).

Given the potential concerns of anomalous fading, it is possible that the TL age of sample #11 represents a minimum estimate for the true burial age of Unit 2. However, the TL age of 46.6 ± 4.2 ka is in agreement with other dating methods applied in Cova del Coll Verdaguer (see sub-sections 4.2.1, 4.2.2, 4.2.4 and 4.2.5). The general concordance between the TL age and these associated independent age estimates suggests that any potential systematic underestimation caused by anomalous fading is likely to fall within the existing 2σ analytical uncertainty range (i.e., ±8.4 ka). Alternatively, the age underestimation associated with anomalous fading could have been masked by the opposing effects of insufficient bleaching. The latter is ultimately difficult to assess at the multiple-grain scale (Arnold and Roberts, 2009; Arnold et al., 2013) and would necessitate single-grain OSL dating to be resolved definitively (Arnold et al., 2013; Demuro et al., 2015, 2013). In the meantime, and on the basis of available evidence, we interpret the TL chronology of sample #11 as a close minimum age estimate for the accumulation of Unit 2, and most likely a reliable age estimate within the associated 2σ analytical uncertainties.

4.2.4. ESR dating

Thirteen samples were collected from Cova del Coll Verdaguer (Tables 5 and 6). Five were sediments (#13, #15, #19, #23 and #24) from different parts of the stratigraphic sequence indicated in Table 6. Sample #16 is a shaft fragment of a ungulate limb bone, and the other seven samples are mammal teeth identified as *Cervus elaphus* (samples #12, #17, #18, #20, #21 and #22) and *Capra pyrenaica* (sample #14). Of these, only three (#12, #21 and #22) yielded enough enamel to at least attempt dating.

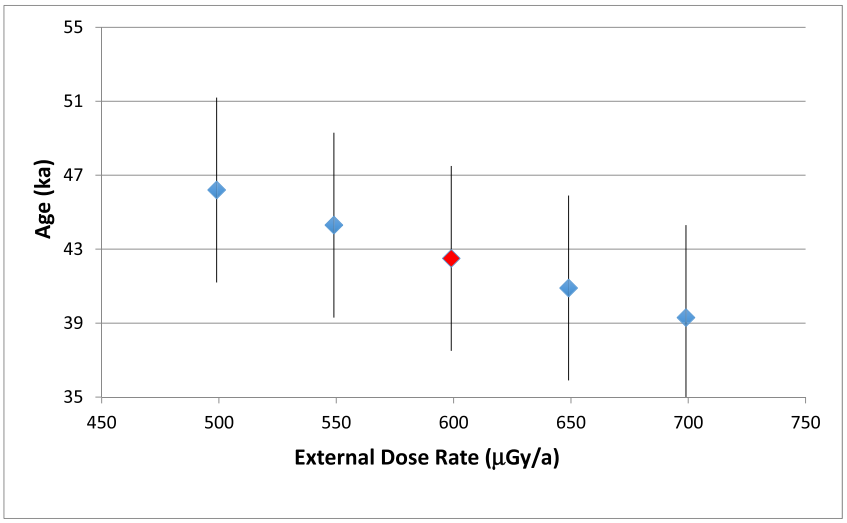

Fig. 4. The effect of changing external dose rate assumptions (soil chemistry and/or water content) on ESR LU age calculations. For a cave environment only changes in water content are likely to be significant. The range shown in the figure goes from 40% water (muddy bog) to 10% (very arid). Error bars are 1σ; central point is as-reported age and external dose rate.

Sample #22 (M1 of *Cervus elaphus*) yielded eight subsamples of which four were completely dated, while one lacked only the NAA for the enamel. The average LU age of the completed samples is 46.4 ± 2.6 ka BP. The LU age is usually the most reliable model; however, even this age depends significantly on assumptions about the environment. The external dose rate was derived from samples #24 and #23. The water content of the samples were estimated at 25%, quite damp but not water-saturated. Fig. 4 shows the effect on the calculated age of different external dose rates.

Sample #21 is also an M1 or M2 molar from *Cervus elaphus*. Six sub-samples were obtained from this tooth, with four being completely dated. One sub-sample required more additive dose measurements and NAA on the enamel. The average LU age is 43.9 ± 3.0 ka, while the external dose rate was derived using the same factors as for sample #22.

The third sample is #12 and corresponds to a premolar P3 of a *Cervus elaphus*. Because of the small size of this tooth, we dated just one single sample. ESR results suggest an LU age of 46.1 ± 7.4 ka, a similar age to that of the other samples.

All three samples provide ESR ages consistent with results obtained by other methods (sub-sections 4.2.1, 4.2.2 and 4.2.3). According to their stratigraphic position, we would expect the ESR samples of Unit 3 to be older than those in Unit 1, but they are statistically indistinguishable.

4.2.5. AAR dating of shells

Four samples were collected, two from Unit 1 and two from Unit 2. The sample ID for each stratigraphic unit and their ages are included in Table 7. The mean D/L values of aspartic acid and glutamic acid in the gastropods from Units 1 and 2 are shown in Table 7, together with their ages. The estimated age of a single stratigraphic unit is the average of the age estimates obtained for each amino acid D/L value of the samples from that unit, and the age uncertainty quoted in this study is the standard deviation of all the age estimates obtained from the D/L values of the samples of each site.

The AAR results were significant and we did not observe any unusual results. In line with Kaufman (2006), we used the cutoff value of 0.8 for the concentration of L-Ser with respect to that of L-aspartic acid to determine anomalous samples, given that Ser

Table 1
Results alpha spectrometric U-series dating of speleothems of the Cova del Coll Verdaguer (1σ confidence interval).

ID	Unit	Site #	Lab#	Material	U ppm	Th ppm	$^{234}U/^{238}U$	$^{230}Th/^{232}Th$	$^{230}Th/^{234}U$	Age yr
2	UFU	6408	6206	Flowstone	0.26	n.d.	1.05 ± 0.02	*****	0.16 ± 0.01	19,262 + 678/-674
3	UFU	6409	3207	Flowstone	1.24	0.05	1.03 ± 0.01	10.8 ± 0.48	0.15 ± 0.00	17,373 + 422/-420
4	UFU	6410	6306	Flowstone	0.01	0.01	1.07 ± 0.03	6.7 ± 0.6	0.14 ± 0.01	15,856 + 728/-723
6	UFU	6411	6106	Carbonates	0.14	0.01	0.98 ± 0.04	8.96 ± 0.78	0.30 ± 0.01	38,347 + 2,285/-2,205

Table 2
MC-ICPMS U-series dating of speleothems of speleothems of the Cova del Coll Verdaguer (2σ confidence interval). All ratios are activity ratios calculated from isotope concentration ratios using decay constants according to Jaffey et al. (1971) (λ238), Cheng et al. (2000) (λ234 and λ230)·and Holden (1990) (λ232).

ID	Unit	Site #	Lab#	Material	^{238}U [ng/g]	^{232}Th [ng/g]	$^{230}Th/^{232}Th$	$^{230}Th/^{238}U$	$^{234}U/^{238}U$	Age [ka] uncorrected	Age [ka] corrected
1	UFU-Top	6419	UEVA 855	Flowstone	225.8 ± 2.1	44.6 ± 0.4	1.49 ± 0.02	0.0964 ± 0.0014	1.0413 ± 0.0023	10.6 ± 0.2	5.0 ± 2.9
5	UFU	6420	UEVA 1027	Flowstone	245.5 ± 2.0	0.492 ± 0.007	211 ± 3	0.1382 ± 0.0015	1.1120 ± 0.0024	14.5 ± 0.2	14.4 ± 0.2
7	LSU	6421	UEVA 843	Stalagmite	210.5 ± 1.8	57.0 ± 0.4	6.88 ± 0.03	0.6097 ± 0.0030	1.0250 ± 0.0024	98.2 ± 0.9	90.4 ± 4.0

Age calculation is based on $\left(\frac{^{230}Th}{^{238}U}\right)(T) = (1 - e^{-\lambda_{230}T}) + \left(\frac{^{234}U}{^{238}U}(T) - 1\right)\frac{\lambda_{230}}{\lambda_{230}-\lambda_{234}}(1 - e^{-(\lambda_{230}-\lambda_{234})T})$ where T is the age of the sample.

The degree of detrital ^{230}Th contamination is indicated by the measured $^{230}Th/^{232}Th$ activity ratio and corrections were calculated using a $^{238}U/^{232}Th$ activity ratio of 0.8 ± 0.4.

Table 3
Radiocarbon dates of remains of *Pinus sylvestris* recognized in Units 1 and 2 of Cova del Coll Verdaguer.

ID	Unit	Site #	Material	Lab #	Pre-treatment	δ13C	Age yr BP	Cal yr BP (2σ)
8	1	4723	Charcoal (*Pinus sylvestris* type)	OxA-23637	ZR	−23.59‰	37,600 ± 550	42,777-41,177
9	1	6412	Charcoal (*Pinus sylvestris* type)	OxA-23636	ZR	−23.16‰	39,950 ± 650	44,841-42,672
10	2	6413	Charcoal (*Pinus sylvestris* type)	OxA-23638	ZR	−25.68‰	38,00 ± 550	43,020-41,497

Table 4
Thermoluminescence (TL) dating summary (1σ) of a sample collected from Unit 2 of Cova del Coll Verdaguer.

ID	Unit	Site #	Material	Lab #	Method [a]	*a*-value [b]	Total dose rate (Gy/ka) [c, d]	D_e (Gy) [d]	Age (ka) [d]
11	2	6414	Polymineral fine grain sediment (2–10 μm)	MAD-4960	TL (MAAD)	0.17	2.61 ± 0.15	121 ± 8	46.6 ± 4.2

[a] TL equivalent dose (D_e) values were determined using a 'total bleach' multiple-aliquot additive dose (MAAD) protocol.
[b] Alpha effectiveness value used for alpha dose rate calculation, determined using the approach of Zimmerman (1971).
[c] Total dose rate comprises alpha, beta, gamma and cosmic-ray contributions. Beta and gamma dose rates were determined from ^{40}K, ^{238}U and ^{232}Th activities calculated on dried and homogenised, bulk sediment samples using a combination of beta counting and thick source alpha counting. The conversion factors of Nambi and Aitken (1986) were used to derive dose rate estimates from measured activities.
[d] Mean ± total uncertainty (1σ or 68% confidence interval), calculated as the quadratic sum of the random and systematic uncertainties.

Table 5
ESR ages of samples from Cova del Coll Verdaguer (1σ). Only three samples had sufficient enamel. *U content is estimated.

ID	Unit	Site #	Lab #	Material	AD(Gy)	Uen(ppm)	Uden(ppm)	Ucem(ppm)	EU (ka)	LU (ka)
12	1	902	ET32	*C. elaphus* P3	66.07 ± 10.20	1.00*	38.78	19.39	30.3 ± 4.8	46.1 ± 7.4
14	1	711		*C. pyrenaica* M1	Failed					
16	2	4871		Bone shaft	Failed					
17	2	5366		*C. elaphus* I	Failed					
18	2	4889		*C. elaphus* DP2	Failed					
20	3	4303		*C. elaphus* DP3	Failed					
21	3	5555	ET27	*C. elaphus* M1-M2	58.12 ± 2.5	1.48	27.66	12.83	31.6 ± 1.7	43.9 ± 3.0
22	3	5686	ET33	*C. elaphus* M1	55.6 ± 2.4	1.25	34.96	19.42	29.6 ± 1.4	46.4 ± 2.6

Table 6
NAA analyses of sediment samples from Cova del Coll Verdaguer. Results for 'N/A' samples have not been returned.

ID	Unit	Site #	Lab #	U(ppm)	Th (ppm)	K(%)	Water content	Dose rate (mGy/a)
13	1	4905	N/A					N/A
15	1	4908	N/A					N/A
19	2	4847	N/A					N/A
23	3	6372	VER13	2.35 ± 0.02	7.74 ± 0.19	1.097 ± 0.03	25% ± 5%	0.681 ± 59
24	3	4910	VER14	2.17 ± 0.02	5.49 ± 0.14	0.747 ± 0.02	25% ± 5%	0.518 ± 50

Table 7
Aspartic acid (Asp) and glutamic acid (Glu) D/L values for gastropod shells together with numerical ages of the archaeological levels of Cova del Coll Verdaguer (2σ).

ID	Unit	Site #	NR	Lab #	Material	Weight (mg)	D/L Asp	D/L Glu	Age (yr)
25	1	6415	3	6022 to 6024	*C. nemoralis*	12.3 to 20.5	0.433 ± 0.001	0.194 ± 0.016	50,055 ± 4,359
26	1	6416	8	6031 to 6038	*C. nemoralis*	8.1 to 21.8	0.428 ± 0.029	0.211 ± 0.017	52,950 ± 9,041
27	2	6417	3	6028 to 6030	*C. nemoralis*	10.0 to 15.1	0.424 ± 0.032	0.225 ± 0.030	55,175 ± 13,343
28	2	6418	4	6025 to 6028	*C. nemoralis*	8.3 to 10.2	0.438 ± 0.011	0.220 ± 0.017	56,137 ± 6,115

decomposes rapidly, and excessive amounts would indicate contamination by modern amino acids. Within their large uncertainties, the AAR results give slightly older ages than those obtained by U-Th, 14c and ESR techniques.

4.3. Stone tools

The lithic assemblage is made up of fourteen artefacts. All the stratigraphic units yielded lithic remains, although most of them correspond to Unit 2 (NR = 6; 43%) and the boundary between Units 1 and 2 (NR = 2; 14%). Three artefacts (21%) were found in Unit 3 and two in Unit 1 (14%). Finally, one artefact (NR = 1; 7%) dropped from the section, its stratigraphic provenience being unknown. Artefact size is highly variable and ranges from 26 × 22 × 8 mm to 62 × 33 × 14 mm. In particular, the total absence of flakes smaller than 20 mm and debris should be stressed.

With the exception of a flake fragment made from quartz (Fig. 5.2), flint is clearly the dominant raw material. Most flint artefacts (NR = 10) display an intense white patina. In addition, one artefact from Unit 2 shows a slightly abraded dorsal surface (Fig. 5.14), while another artefact from Unit 2 exhibits evidence of crazing which suggests thermal damage (Fig. 5.8). All the artefacts are flakes (NR = 12; 86%) or flake fragments (NR = 2; 14%). Neither cores nor retouched implements have been identified. Two flakes (Fig. 5.13 and 5.14) exhibit some marginal and discontinuous removals along one edge, but these seem unintentional and are

probably related to use-wear. There are no blades, but most flakes (NR = 9; 64%) are longer than they are wide and two of them can be considered elongated flakes (length-to-width ratio higher than 1.5).

In general, flake butts are plane and unprepared. Only one flake shows a facetted striking platform. Most artefacts (NR = 11; 79%) do not exhibit cortex in their dorsal surfaces. It is particularly noteworthy that flakes with asymmetric transversal profiles are common. Six flakes are clearly characterised by presenting a cutting edge opposed to an abrupt back. Of these, three are *débordant* flakes (Fig. 5.5, 7 and 8), two are naturally backed flakes (Fig. 5.10 and 11) and one can be classified as a pseudo-Levallois point (Fig.5.12). Another flake with a very wide, thick butt opposed to a distal edge can also be included in the group of artefacts with asymmetric profile (Fig. 5.9).

The technological and cultural contextualization of the lithics is hampered by the small number of artefacts and the absence of culturally diagnostic items. The production of *débordant* flakes and pseudo-Levallois points is common in the centripetal methods typical of Mousterian technologies. The small size of the assemblage and the metrical and morphological characteristics of the artefacts suggest that most of them were not produced *in situ* but rather introduced from outside. Small flakes and debris are entirely absent, which indicates that knapping activities were not common inside the cave. In addition, the asymmetrical profile of most flakes

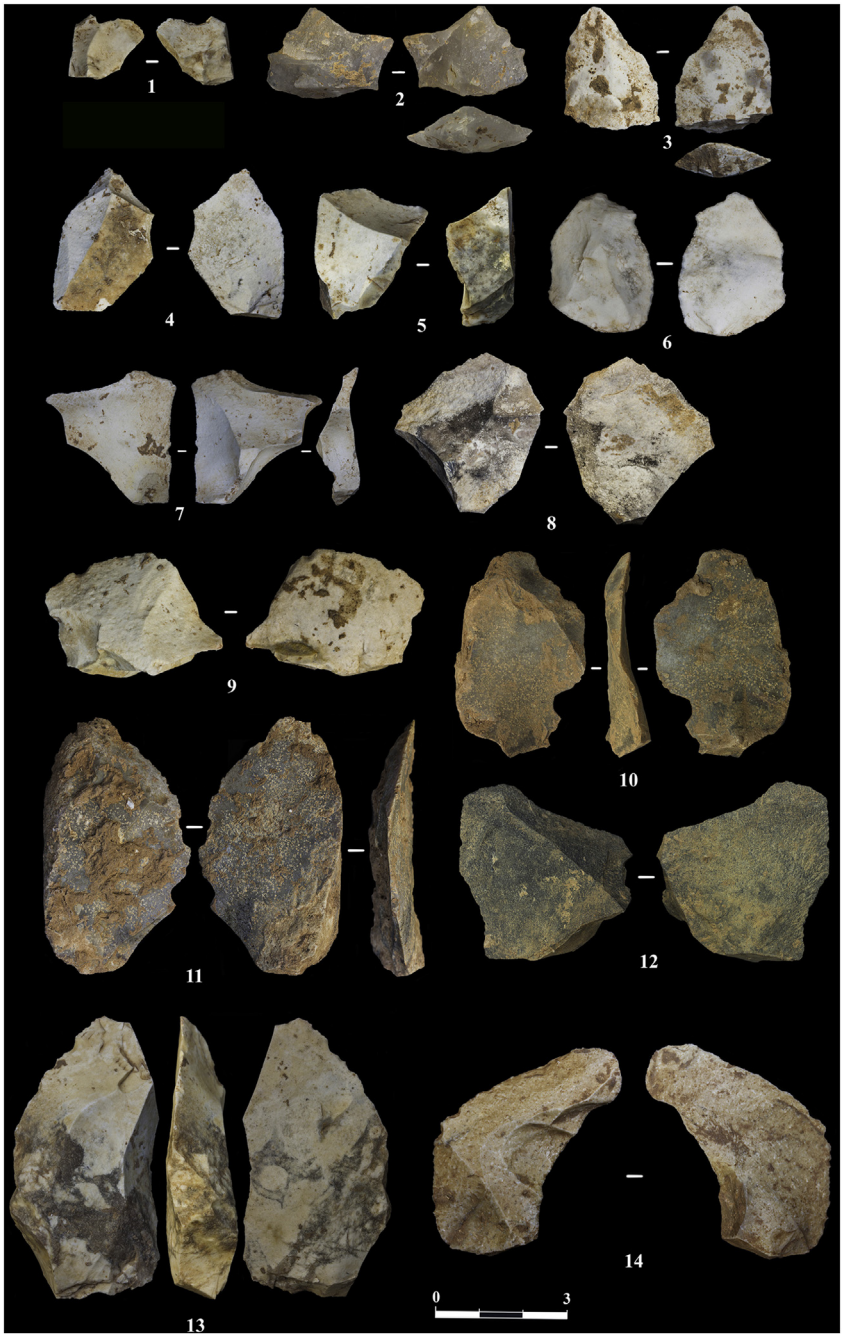

Fig. 5. Lithic artefacts from the Cova del Coll Verdaguer. 1: Flint flake fragment. 2: Quartz flake fragment. 3, 4, 6 and 9: Ordinary flint flakes. 5, 7 and 8: *Débordant* flakes. 10–11: Naturally backed flakes. 12: Pseudo-Levallois point. 13 and 14: Flakes with marginal and discontinuous removals on one edge.

is in keeping with the type of blanks normally selected for transport at the nearby site of Abric Romaní (Spain) (Vaquero et al., 2012). This selection for transport was may be due to the ergonomic properties (Beyries and Boëda, 1983) of the artefacts opposing a back to a cutting edge – *débordant* flakes, naturally backed flakes. If this is the case, high percentages of these artefacts in lithic assemblages formed primarily by the accumulation of transported items, as would seem to be the case at Cova del Coll Verdaguer, should be expected.

Although the deposition of transported artefacts is the dominant formation process, knapping was not entirely absent, as it shown by the refitting of two flakes (Fig. 6). These are two naturally backed flakes that were detached following the same axis of debitage. One of the flakes was found in Unit 2 (square D7), and the other in Unit 3 (square H8). This refit indicates that a short reduction sequence was carried out in or around the excavated area. The two refitted flakes are among the few artefacts without white patina, which suggests that they were less exposed to post-depositional processes of alteration.

4.4. Faunal remains and vegetation

4.4.1. Large mammals

Ten species of large mammals were identified (Fig. 7 and Table 8) from a total of 1,721 remains from the three stratigraphic units. Ungulates are the most abundant taxa in the assemblage (NISP = 1,529, MNI = 42) represented by five species (*Cervus elaphus*, *Capra pyrenaica*, *Equus caballus*, *Capreolus capreolus*, *Bos/Bison*). Of the ungulate remains, 54% are non-identifiable fragments and were classified according to body size (small, medium or large).

Five species of carnivore (*Ursus arctos*, *Felis silvestris*, *Lynx pardinus*, *Vulpes vulpes* and *Meles meles*) were identified, corresponding to a NISP of 179 and 22 individuals. The most abundant carnivore in the three units is the brown bear, represented primarily by yearlings and neonate specimens (MNI = 10). The yearlings are represented by shed deciduous canines, replaced around the 14th month of life. Lynx and red fox are also present throughout the sequence, with a MNI of 5. Wildcat and badger are each represented by just one cranial remain. Although bones of hyena were not founded, their presence is demonstrated by the presence of coprolites and gnawing marks recognized in bones (Sanz et al., 2016).

Fig. 6. Refit of two flint flakes, corresponding to nº 10 and 11 in Fig. 5.

The assemblage of Cova del Coll Verdaguer is primarily a carnivore den, the most important activity therein being related to hyenids (Sanz et al., 2016). The gnawing patterns observed on bone specimens is typical of that described for extant and fossil hyenid accumulations (Villa et al., 2010), with the presence of partly digested bones, cylinders and shaft fragments and rare epiphysis (Sanz and Daura, 2017; Sanz, 2013). The bear, the most abundant carnivore at the site (Fig. 7.8 and 7.9), is not expected to bring carcasses into the denning site (Sala and Arsuaga, 2013); hence, the taphonomic evidence points to hibernating females with cubs inside the cave (Andrews and Turner, 1991). Furthermore, a total of 277 coprolites were identified and grouped into three categories: Morphotype 1 (NR = 209) corresponds to hyena; Morphotype 2 (NR = 72) to medium or small carnivore (e.g. wolf, lynx, or fox) and Morphotype 3 (NR = 11) to large carnivore (e.g. bear) (Sanz et al., 2016) (Fig. 7.14 and 7.15). In general, human action is not observed on bones, since no cut-marks or any other anthropogenic damage were observed. Only a few burned bones (NR = 7) (Fig. 7.12 and 7.13) in all units (Unit 1 NR = 4; Unit 2 NR = 2; Unit 3 NR = 2) were recovered.

4.4.2. Microfauna

The small mammal assemblage corresponds to 174 identified specimens and 117 individuals and is composed of 14 identifiable taxa (Table 8): two insectivores (*Talpa europaea* and *Crocidura russula*), three bats (*Rhinolophus* sp., *Myotis* gr. *myotis-blythii* and *Myotis* sp.) and nine rodents (*Arvicola sapidus*, *Chionomys nivalis*, *Iberomys cabreraee*, *Microtus arvalis*, *Microtus agrestis*, *Microtus* (*Terricola*) *duodecimcostatus*, *Apodemus sylvaticus*, *Eliomys quercinus* and *Sciurus vulgaris*). The assemblages from each of the main stratigraphic units provide evidence of different paleoenvironments. Unit 3 is dominated by species associated with open meadows, such as *Microtus arvalis*, *Iberomys cabrerae* and *Microtus* (*Terricola*) *duocedimcostatus*. In Unit 2, the open-meadow species are still dominant, but this unit denotes a slight increase in the taxa associated with woodland environments, such as *Apodemus sylvaticus*. Finally, in Unit 1, there is a marked increase in the species associated with forest formations, such as *A. sylvaticus* and *Eliomys quercinus* (Table 8).

4.4.3. Birds

Among the faunal remains, sixteen were identified as bird bones, eleven of these being ascribed to seven avian taxa (Table 8). The seven species recorded (one, the dove, with some doubts regarding its specific attribution) are among present-day Iberian birds. Three remains belong to a partridge of the genus *Alectoris*. The species within this genus reach the same size and their skeletal features are indistinguishable (Fick, 1974). The crag martin is the largest bird of its family and has the most robust humerus among European hirundinids. The humeri of *Coccothraustes coccothraustes* and *Loxia* are almost identical, but the bicipital crest is wider in the region of the ventral tubercule in the latter genus.

In general, the species recovered at the site currently inhabit this region, with the exception of the rook and the yellow-billed chough. The rook's distribution is currently restricted to a small area of the northern central Spain. The yellow-billed chough is found today only in high mountain areas, but it appears in the Pleistocene deposits located at low altitudes at all heights. As such, its presence is of no special significance for the

Fig. 7. Large mammal remains. 1: Ibex (*Capra pyrenaica*) skull. 2: Roe deer (*Capreolus capreolus*) mandible. 3–4: Infantile horse (*Equus caballus*) mandible and distal limb in anatomical position. 5-6-7: Red deer (*Cervus elaphus*) maxilla, immature and mature mandible. 8-9: Brown bear (*Ursus arctos*) deciduous canines and mandible. 10: Lynx (*Lynx pardinus*) mandible. 11. Fox (*Vulpes vulpes*) mandible. 12–13: Calcined bone fragment. 14–15: Morphotype 1 and 2 coprolite.

palaeoenvironmental reconstruction (Sánchez Marco, 2004; Sánchez-Marco, 1996). Cova del Coll Verdaguer presents a poorer taxonomic composition of birds, but one that coincides closely with the neighbouring deposit at Terrasses de la Riera dels Canyars, dated at 39.6 ka cal BP (Daura et al., 2013) and located 12 km to the south-east of the study site. The *Alectoris* partridge, the hawfinch and both choughs are present at both archaeological sites. The *Alectoris* species lives in open areas with scrub.

4.4.4. Malacology

The malacological diversity increases from the bottom to the top of the stratigraphic sequence, with five species being identified in Unit 3, nine in Unit 2 and 10 in Unit 1 (Table 8). Nevertheless, in all three units, the same four species are dominant. *Theba pisana* is the most abundant malacofauna, representing between 41.6 and 50.1% of the shells collected, whereas *Pseudotaecha splendida* is present in percentages ranging between 30.1 and 40.2%. The remaining two species are much less frequent: *Xerocrassa penchinati* (5.6–11.2%) and *Cepaea nemoralis* (4.7–7.7%).

Theba pisana is today one of the most common snails in European Mediterranean coastal regions. It usually inhabits coastlands or sandy habitats in warm climates, dwelling in grasses, shrubs or succulent plants. However, it can also be found in more northern European sites. *Pseudotaecha splendida* is typically found in dry meadows, shrubs and rocks covered by vegetation, old walls and wine slopes, up to an altitude of 1200 m. It is limited to the east of Spain and south of France. *Xerocrassa penchinati* dwells under stones, preferably in highlands and mountains, and its distribution is limited to the east of Spain and the Pyrenees. Finally, *Cepaea nemoralis* mainly inhabits shrubs and open woods on plains, highlands, dunes and sites with plants, and has a western-central European distribution (Adam, 1960; Bech, 1990; Borredà et al., 2010; Cadevall and Orozco, 2016; Haas, 1929; Locard, 1894; Ruiz et al., 2006; Welter-Schultes, 2012); however, this taxon has been

Table 8
Faunal species represented in Cova del Coll Verdaguer.

	Unit 1		Unit2		Unit 3		Total	
	NISP	MNI	NISP	MNI	NISP	MNI	NISP	MNI
Mammalia								
Carnivora								
Felis silvestris	1	1					**1**	**1**
Lynx pardinus	14	1	13	1	73	2	**100**	**4**
Ursus arctos	7	3	15	5	16	3	**38**	**11**
Vulpes vulpes	7	1	3	1	28	2	**38**	**4**
Meles meles			1	1			**1**	**1**
Carnivora undet.	1				13		**14**	
Perissodactyla								
Equus caballus	9	1	51	3	47	4	**107**	**8**
Artiodactyla								
Bos/Bison	1	1					**1**	**1**
Capra pyrenaica	26	1	22	3	92	4	**140**	**8**
Capreolus capreolus	5	3	6	1	12	1	**23**	**5**
cf. *Cervidae/Caprinae*	24		14		55		**93**	
Cervus elaphus	113	7	67	5	156	8	**336**	**20**
Ungulates per body size								
Small	128		71		82		**281**	
Medium	182		118		233		**533**	
Large	6		1		8		**15**	
Lagomorpha								
Leporidae*	106	55	20	10	41	23	**167**	**88**
Soricoforma								
Talpa europaea	6	2	2	1	1	1	**9**	**4**
Crocidura russula	1	1	1	1			**2**	**2**
Chiroptera								
Rhinolophus sp.	1	1					**1**	**1**
Myotis gr. *myotis-blythii*	2	2			1	1	**3**	**3**
Myotis sp.	1	1					**1**	**1**
Rodentia								
Arvicola sapidus	1	1	2	1	1	1	**4**	**3**
Chionomys nivalis	1	1			4	2	**5**	**3**
Iberomys cabrerae	8	5	12	10	14	9	**34**	**24**
Microtus arvalis	11	6	9	5	26	14	**46**	**25**
Microtus agrestis	1	1	4	3	7	6	**12**	**10**
M. arvalis-agrestis	1	1	1	1			**2**	**2**
Microtus (*Terricola*) *duodecimcostatus*			5	3	10	6	**15**	**9**
Apodemus sylvaticus	16	10	11	4	1	1	**28**	**15**
Eliomys quercinus	6	4	2	1	5	5	**13**	**10**
Sciurus vulgaris	1	1	1	1			**2**	**2**
Aves								
Galliformes								
Alectoris cf. *rufa*	2	1	1	1			**3**	**2**
Columbiformes								
Columba livia/C. oenas			1	1			**1**	**1**
Passeriformes								
Ptyonoprogne rupestris					1	1	**1**	**1**
Coccothraustes coccothraustes	1	1					**1**	**1**
Corvus corone/C. frugilegus	1	1					**1**	**1**
Pyrrhocorax pyrrhocorax	2	1					**2**	**1**
Pyrrhocorax graculus	2	1					**2**	**1**
Gastropoda								
Pulmonata								
Bithynia tentaculata		2						**2**
Galba truncatula				2				**2**
Abida polyodon		9		10		3		**22**
Discus rotundatus		2		7				**9**
Sphincterochlia af. baetica		51		5		7		**63**
Suboestophora tarraconensis		12		2				**14**
Xerocrassa penchinati		96		94		45		**235**
Cepea nemoralis		132		44		19		**195**
Ibirellus hispanicus		9						**9**
Pseudotaecha splendida		692		261		156		**1,109**
Theba pisana		715		424		170		**1,309**

*Leporids were not analysed; however, cranial remains were used to estimate the MNI based on site inventory.

commonly recorded in temperate, humid conditions (Ballesteros et al., 2017; Mazon et al., 1987).

None of the most abundant species (*P. splendida* and *T. pisana*) in the samples is a cave dweller. With the exception of *X. penchinati*, they are characteristic of dry open environments, generally associated with sclerophyllous vegetation. Their presence inside the cave can be explained by wind or water transportation from the surrounding area (which would have provided suitable habitats), or alternatively by human transport. However, the complete shells do not show any evidence of human activity.

Table 9
Charcoal fragments identified in Cova del Coll Verdaguer.

Taxa	Unit 1		Unit 2		Unit 3		Total	
	NR	%	NR	%	NR	%	NR	%
Pinus sylvestris type	350	78.3	237	84.0	21	80.8	608	80.5
Pinus sp.	1	0.2					1	0.1
Prunus	48	10.7	11	3.9			59	7.8
Quercus sp. *deciduous*	4	0.9			1	3.8	5	0.7
cf. *Ephedra*			1	0.4			1	0.1
cf. *Prunus*			2	0.7			2	0.3
Undetermined angiosperm	2	0.5	4	1.4			6	0.8
Undetermined conifer	24	5	14	5	2	7.7	40	5.3
indeterminable	18	4	13	4.7	2	7.7	33	4.4
Total	**447**		**282**		**26**		**755**	

4.4.5. Anthracology

The charcoal assemblage is very well preserved and presents low values of undetermined fragments (Table 9). However, the results of the anthracological analysis do not enable us to determine the exact origin of the charcoal found in this assemblage. The results are largely homogenous with high values of *Pinus sylvestris* type in all the stratigraphic units (Unit 1: 78.3%; Unit 2: 84%; Unit 3: 80.8%) (Table 9). This taxon includes different species of mountain pines, including *Pinus sylvestris*, *Pinus nigra* and *Pinus uncinata*, which show the same wood anatomy and cannot be distinguished (Schweingruber, 1990). *Prunus* is also present in both units, presenting a slightly higher value in Unit 1 (10.7%) than in Unit 2 (3.9%). *Prunus* genus includes several species that share the same wood anatomy. However, some of their characters allow us to classify this genus in different types (Heinz and Barbaza, 1998). Most of the *Prunus* identified in Cova del Coll Verdaguer show a diffuse pore pattern and multi-seriated ray cells, which could correspond to *Prunus spinosa/mahaleb* type. In contrast, fragments from Unit 2 present bi- or tri-seriated ray cells that could correspond to *Prunus avium/padus* type. This suggests that there was more than one species of *Prunus* growing in the area. Finally, *Quercus* sp. deciduous has been identified in Units 1 and 3 with a very low presence (0.8%) (Table 9). This taxon includes all the deciduous oaks that cannot be distinguished on the basis of their wood anatomy.

4.4.6. Palynology

Ten coprolites were analysed, four of which were palynologically sterile (Fig. 8). There is no discernible palynostratigraphic pattern following the stratigraphic succession of the Cova del Coll Verdaguer site. With the exception of one sample (Site Inv. # 1753), dominated by Poaceae, the pollen assemblages of the analysed coprolites show the prevalence of *Pinus*, with percentages ranging between 50 and more than 90 (Site Inv. # 803). Other relatively abundant types (10%) include Poaceae, Cichorioideae, Asteroideae, *Artemisia* (Site Inv. # 4154) and *Juniperus*. Minor, although, ecologically significant, accounts are found for deciduous and evergreen *Quercus*, *Alnus, Betula, Acer, Buxus, Prunus,* and *Olea*. Based on taphonomic experience with hyena and canid coprolites (Carrión et al., 2008), this disparity in the composition of pollen spectra seems to reflect the presence of several different habitats in the surrounding area, with forested areas clearly dominated by pines – especially at the local scale, and Poaceae/*Artemisia* steppe-like landscapes with sparse trees and shrubs. It is worth remarking, however, that the occurrence and land cover of thermophilous flora during this part of MIS 3 in the region are less important than in lower latitudes of the Iberian Peninsula (Carrión and Leroy, 2010; Carrión, 2002; González-Sampériz et al., 2010).

5. Discussion

5.1. Site formation and chronostratigraphy

The speleogenesis of Cova del Coll Verdaguer can be summed up in four main phases, based on the cave history and the stratigraphic sequence. Episodes 1 and 2 correspond to a period predating the opening of the cave and include a major collapse of larges blocks

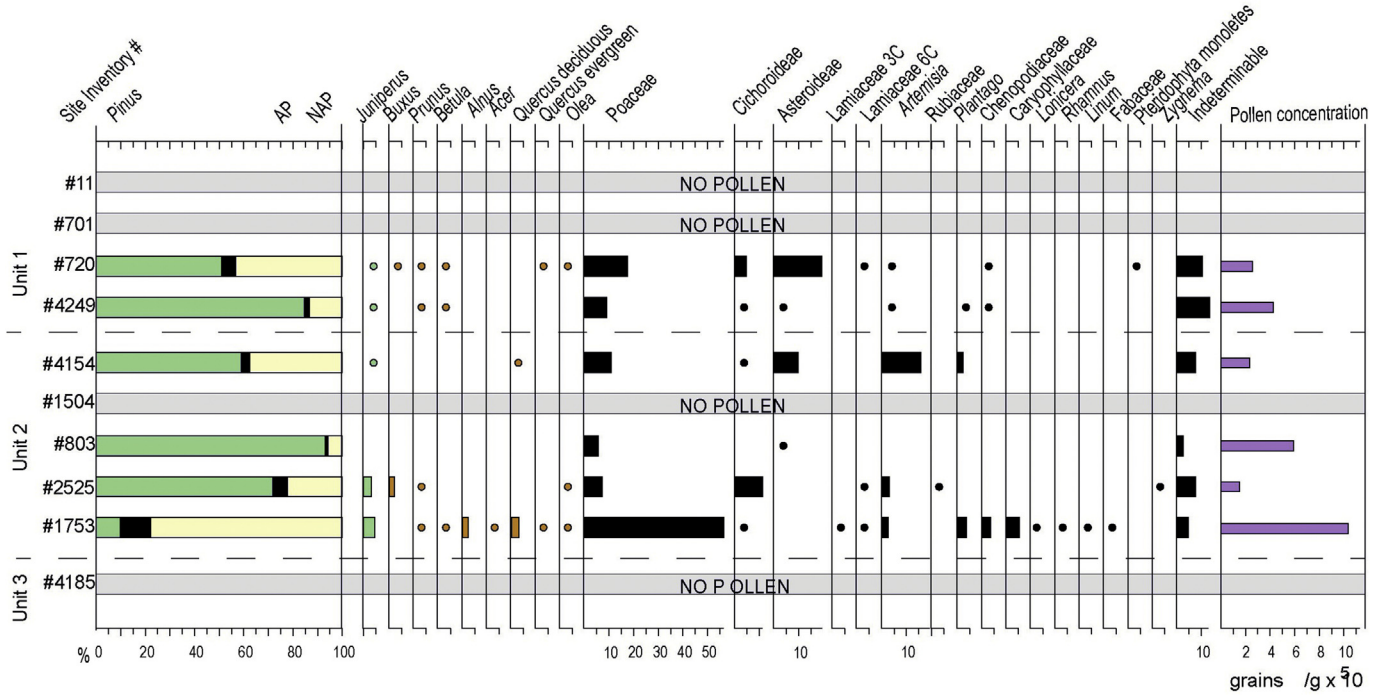

Fig. 8. Pollen content of the hyena coprolites recognized in the three main stratigraphic units.

from the roof (LBU) and speleothem formation (LSU) above. Indeed, several caves located in the same area could be indicative of a more generalized process operating throughout the region (Daura, 2008).

Episode 3 is represented by the accumulation of the archaeological deposit (CDU) and the last layer of the calcite crust from the stalagmite originating from the LSU, formed before the accumulation of the CDU (Unit3), which buried the stalagmite. This dates to 90.4 ± 4.0 ka, and provides a maximum age for the entire archaeological deposit and a minimum age for Episodes 1 and 2. Episode 4 corresponds to the upper speleothem formation (UFU) and occurred between 19.3 ± 0.7 and 5.0 ± 2.9 Ka BP.

The 3-m thick sedimentary CDU sequence of Episode 3 at Cova del Coll Verdaguer was deposited between 34.2 and 90.4 ka. This chronological range of the sequence is given primarily by U-Th and radiocarbon dating. The flowstone at the top of the sequence is dated by U-Th disequilibrium to an age of ~of 34.2 at 2σ (or 36.2 ka at 1σ confidence), which represents a minimum age estimate for the entire deposit. The maximum age is provided by dating the buried stalagmite. In contrast, the charcoal dates lie at the limit of the radiocarbon method and are difficult to interpret owing to problems of ensuring reliable decontamination. Unit 1 samples are statistically indistinguishable, providing an age of 42.8–41.2 ka cal BP for the top and 44.8–42.7 ka cal BP for the base, that is, a combined range between 41.2 and 44.8 ka cal BP.

The radiocarbon age provided by the Unit 2 sample, i.e., 41.5–43.0 ka cal BP, is consistent with the range provided by the Unit 1 samples. The TL and ESR ages provide additional constraints on the infill phases and enable multi-technique assessments to be made of the dating consistency. The TL and ESR results are broadly consistent with radiocarbon and U-Th dating and the reported ages are in accordance with their stratigraphic position. The AAR ages obtained in the Unit 1 samples (50–53 ka) are relatively older than the range established for Unit 1 by other techniques (41–48 ka).

The chronology of Unit 3 is more difficult to determine, given that according to the radiocarbon results for Units 2 and 1, it appears to lie beyond the limits for radiocarbon dating. The application of the LU model for ESR datings seems to be more suitable than the EU model because the ages provided by the former are in closer agreement with the results of other chronological techniques; however, the EU model is able to predict a minimum age for the deposit. The chronology of Unit 3 based on ESR measurements is not straightforward given that their large 2σ confidence interval overlaps the entire deposit. Despite this, there are two possible interpretations of the ESR chronology: i) by considering each ESR sample independently, this gives a chronology of 38–53.5 ka for Unit 1, and ages of 40.9–46.9 ka or 43.8–49 ka at 1σ for Unit 3; or ii) considering that all three ESR samples taken together represent the same model for the U-uptake history, which gives the same chronological phase of between 38 and 53.5 ka.

In short, the stratigraphic sequence of Cova del Coll Verdaguer could represent a rapid sedimentation process that occurred between 34.2 and 90 ka, based on U-Th dates. If we consider all the dating methods applied and take the DCU unit to be a single deposit, the sedimentation of Cova del Coll Verdaguer probably occurred between 34 and 56 ka.

5.2. Palaeoenvironmental reconstruction

The Cova del Coll Verdaguer sequence is associated with a period from the beginning of MIS 3, including D-O cycles from 17 to 12, as well as the Heinrich Stadial 5 (see Fig. 9). According to the results of the pollen analyses, this period alternated between periods of forest development and the expansion of semi-arid and steppe biomes depending on the sequence of warming and cooling events, respectively, of the sea surface temperatures (Fletcher and Sánchez Goñi, 2008; Harrison and Sanchez Goñi, 2010).

In general, the vegetation record in the NE of Iberian Peninsula during the MIS 3 (Allué et al., 2017b; Carrión, 2002; Daura et al., 2013; González-Sampériz et al., 2010) points to a landscape dominated by conifers (*Pinus sylvestris* type and *Juniperus*) in association with components of evergreen and deciduous species (*Quercus*, *Corylus*, *Alnus*, *Tilia*, *Buxus*, *Acer*, *Sorbus domestica*, *Rhamnus Prunus, Fagus).* The results from Cova del Coll Verdaguer match the records of other Pleistocene sites (e.g. Abric Romaní, Cova de l'Arbreda, Cova Gran, Terrasses de la Riera dels Canyars) in which charcoal and pollen (e.g. Abric Romaní) data point to the predominance of arboreal coverage in the vegetation (Allué et al., 2017a; Burjachs et al., 2012). The charcoal data from Cova del Coll Verdaguer indicate the predominance of *Pinus sylvestris* type and a low taxa diversity. This pattern has also been reported for other sequences in the NE of the Iberian Peninsula, including Abric Romaní, Arbreda and Canyars (Allué et al., 2017a, 2017b; Daura et al., 2013; Ros, 1987). The predominance of *Pinus sylvestris* type is also evident in the anthracological records of sites in the SE of the Iberian Peninsula (Badal et al., 2012) and at various sites in northern Spain (Uzquiano, 2008; Uzquiano et al., 2012).

Based on ecological and biogeographical data, *Pinus nigra* appears in low altitudes of coastal areas (Badal et al., 2012; Vernet, 2006). This pine was probably widespread across the Mediterranean basin during the Pleistocene (Alejano and Montes, 2006; Badal et al., 2012; Roiron et al., 2013; Vernet, 2006) and the trees in the vicinity of Cova del Coll Verdaguer may well have been of this species. However, any differentiation between mountain pine species in Cova del Coll Verdaguer is not yet possible and further analyses need to be carried out in order to identify their specific distribution.

The pines documented in the palynological and anthracological records of Cova del Coll Verdaguer are likely to have formed groves, especially on the slopes near the cave. The rest of this habitat was probably characterised by open, steppe-like vegetation cover with sparse trees and shrubs in lowland areas and in neighbouring valleys (i.e. Sant Ponç and Vallirana -Fig. 1), a similar vegetation pattern to that found in the area today (Fig. 1.2). The presence of both *Quercus* sp. deciduous and *Prunus* indicates the development of mesophilous vegetation, which might be indicative of milder climate conditions. These taxa may have grown within the conifer forests, at the forest limits or in the shaded or narrow valleys of the area. Other anthracological assemblages from the NE Iberian Peninsula also present a predominance of the *Pinus sylvestris* type and the presence of mesophilous taxa at low values (Allué et al., 2017b; Ros, 1987). In the southern latitudes in the Iberian Peninsula, the presence of *Quercus* sp. evergreen in association with *Juniperus* and *Ephedra* alongside the pine forests indicate a more steppic environment (Badal et al., 2012), whereas in the north of the Iberian Peninsula the environment was probably more humid, as shown by the significant presence of *Betula* and *Corylus* (Uzquiano, 2008). This marked vegetation gradient in the Iberian Peninsula is also quite apparent in Cova del Coll Verdaguer, although characterised by a smaller component of thermophilous species. The surroundings of the studied cave probably constituted an ecozone with a highly diverse cover of vegetation influenced by the Mediterranean climate, which would have provided milder conditions within the prevailing cold climate pattern of the MIS 3. However, we cannot rule out that the palaeoclimate studies provide evidence that the MIS 3 involved greater variability, with peaks colder than the temperatures reached in the MIS 2.

The small mammal component of the fauna is in agreement with the floristic data and points to the forested conditions present during the deposition of Units 1 and 2. Indeed, micromammals signal an increase in the arboreal component from the base of the

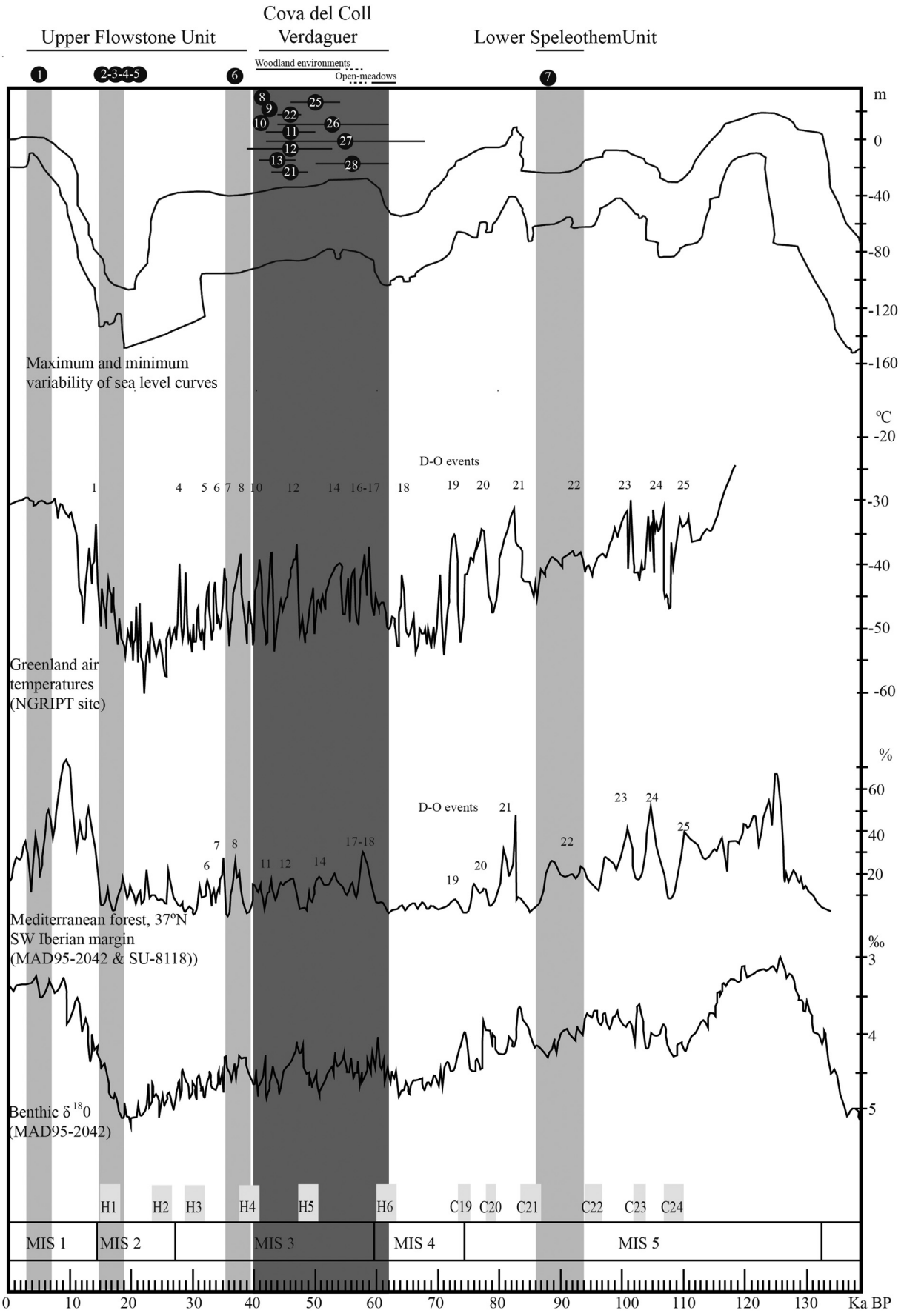

Fig. 9. Schematic, hypothetical palaeoenvironmental reconstruction of Cova del Coll Verdaguer compared to marine isotope stages, maximum and minimum relative sea-level oscillation envelope based on relative sea-level (RSL) curves, Greenland temperature reconstruction, Mediterranean forest reconstruction and benthic foraminiferal d^{18}O (Andersen et al., 2004; Rabineau et al., 2006; Sánchez Goñi et al., 2008).

sequence (Unit 3) to the top (Units 2 and 1). The small mammals present in Unit 3 may be associated with open meadows, but no pollen record has been recovered from Unit 3, while the scarce charcoal data point to forested conditions. However, the pollen sample recovered from the base of Unit 2 (sample #1753) indicates more open, steppe-like conditions dominated by non-arboreal taxa (Poaceae). This sample is distinct from the other vegetation samples, being more similar to the environmental reconstruction inferred from the small mammal component in Unit 3. A single sample of pollen, however, does not indicate anything. Two possible explanation allow us to interpret this palynological sample: (i) if more closely related to Unit 2, the sample points to a landscape that was (at several points in the sequence) a mosaic of pine trees and open meadows depending on local conditions (soil, humidity, slope, etc.) or (ii) if more closely related to Unit 3, the sample signals an open-meadow landscape at the base of the stratigraphic profile.

The large mammal component of the fauna record is consistent with other bioarchaeological records. The most abundant taxa in the assemblage is the red deer (MNI = 20; 32%), an intermediate feeder, presenting a mixed feeding regime on grasses, sedges, leaves, heaths and shrubs (García García et al., 2009; Gebert and Verheyden-Tixier, 2008). In terms of abundance, the deer is followed by the brown bear (MNI = 11; 17%) which is capable of living in a wide variety of habitats (Richards et al., 2008). The diet of the caballine horse (MNI = 8; 13%) is thought to be composed primarily of the herbaceous plants of the grasslands or the open forests on the surrounding slopes. The ibex (MNI = 8; 13%) appears to have been present on the steep-rocky terrain. However, the presence of the roe deer (MNI = 5; 8%) in all three units points to the predominance of a forested environment. In terms of MNI, the woodland herbivores represent 60% of the assemblage, that is red deer (48%) and roe deer (12%). Despite the presence of open landscapes herbivores, such as the horse (19%), the most abundant species identified in the assemblage is in agreement with the scenario presented by the vegetation record, namely that of the forested landscape. A gradual process of increasing forest cover can be observed from Unit 3 to Units 1 and 2. Thus, in Unit 3, the horse and the ibex present the highest values of relative abundance, whereas in Units 1 and 2 there is an increase in woodland taxa, most notably the roe deer.

The gastropod component is indicative of European Mediterranean conditions. Here, the increase in the number of specimens from the base of the sequence to the top could be in line with other palaeoenvironmental indicators. For example, the marked increase in the abundance of the ensemble formed by *Xerocrassa penchinati, Pseudotaecha splendida* and *Theba pisana* from Unit 3 to Unit 1 could be an indicator of warmer and drier conditions. Evidence for this Mediterranean component is further strengthened by the avian remains. For, example, the current distribution of the red-legged partridge defines the bioclimatic Mediterranean area in the Iberian Peninsula and France. The hawfinch is a dweller of forest edges, woodland and shrubs. The remaining species of birds documented at Cova del Coll Verdaguer are typical of rocky crags, and were probably inhabitants of the cave. All the birds represented are associated with these environmental conditions and their remains are present in the cave surroundings (except those of both choughs) which points to slightly cooler conditions than those recorded today.

5.3. The landscape of the last Neanderthals in the NE of Iberian Peninsula

Cave evolution can be diverse and difficult to reconstruct, with several taphonomic studies showing that deposits typically occur in the form of low-resolution palimpsests (Bailey and Galanidou, 2009; Bailey, 2007) or time-averaged deposits. Based on the taphonomic inferences drawn in association with the large mammals here, the assemblage appears to have been accumulated by the same agent/s across the three main units. Carnivores, especially hyenids, are the main biological agents of bone modification and accumulation (Sanz et al., 2016). This means the taxonomical differences across the stratigraphic sequence are not linked to the prey-predator relationship and, presumably, that there is no significant bias between the species recovered and their relative abundances that might be related to environmental factors, i.e. the biomass in the ecosystem (Brugal et al., 1997). Our study of the Cova del Coll de Verdaguer indicates that pine woodlands dominated the NE of the Iberian Peninsula during 45–41 ka, with persistent Mediterranean thermophilous species (stratigraphic units 1 and 2). In contrast, the predominance of open meadows indicated by Unit 3 is associated with a harsher climate. Today, Cova del Coll Verdaguer is ~15 km inland, but at the time of the deposition of the cave sequence, a coastal platform with a width of between 8 and 13 km was emerging in front of the current coastline during the Last Glacial period (MIS 3 and 4), based on the topography and the relative sea-level curves of the Mediterranean sea (Rabineau et al., 2006). The wide littoral platform provided suitable land for resources, migrations and relationships with the south (Levant corridor), the west (Ebro Valley) and the south of France. However, Cova del Coll Verdaguer does not present a significant animal biomass during this period, only the slight dominance of species adapted to open environments (such as the horse) and rocky landscapes (such as the ibex). No cold-adapted large mammal species, such as the woolly rhino or mammoth, have been identified in the sequence, probably signalling that the resources were insufficient to maintain a high biomass of ungulates (Sanz, 2013).

The chronological study of the archaeological and palaeontological context is often imprecise and several models of faunal extinction and dispersion have been constructed on unreliable and fragmentary data, see, for example, Daura et al. (2015) for MIS 5 reconstruction. Chronological adscription and taxonomical identification often present a circular reasoning, and more detailed and better sorted data are required. That said, several studies have suggested models based on both extant and new data in an attempt at clarifying the presence of different taxa. For example, it has been suggested that cold-adapted faunal elements were sporadically present in the Iberian Peninsula from the time of MIS 4 but that it was not until mid-MIS 3 that any expansion occurred (Álvarez-Lao and García, 2010; Álvarez-Lao and Méndez, 2016; Álvarez-Lao et al., 2017; Gómez-Olivencia et al., 2014). In the NE Iberian Peninsula, the sequence of Cova del Coll Verdaguer indicates that neither cold-adapted (i.e. *Mamuthus primigenius* and *Coelodonta antiquitatis*) nor arid-adapted (*Equus hydruntinus*) faunal elements were present. Indeed, a similar pattern of Cova del Coll Verdaguer is observed in layers A to O (i.e. ~40–50 ka) at the Abric Romaní site (Gabucio et al., 2014). In contrast, during the MIS 3 cold-adapted and arid-adapted fauna were present in the Terrasses de la Riera dels Canyars (Daura et al., 2013). There are two possible explanations for these differences. First, the regional landscape comprised a complex mosaic of two distinct biomes depending on the orography, one associated with littoral plains characterised by a steppe-like landscape with enough edible plants to support megafauna, and another associated with mid-altitude, limestone littoral mountains dominated by a boreal forest or a mixed coniferous forest, characterised by low biomass resources with poor edible plants and dispersed herbivore populations. Second, the archaeological and palaeontological sequences represent distinct MIS 3 climate episodes indistinguishable chronologically because of the lower precision of the dating methods. Consequently, the high climate variability is enough to explain the variability in the

paleontological record.

As for any human presence, the scarce lithic assemblage is characterised by the absence of blade production and the presence of *débordant* flakes and one pseudo-Levallois point. These artefacts tend to be common in Mousterian assemblages. The radiocarbon age of Unit I is especially relevant in relation to the Neanderthal presence in this territory until the arrival of modern humans. Until now, the archaeological record showed that the early presence of modern humans occurred, at least, by around 34 ka 14C (or 37.5 cal BP from the nearby site of Terrasses de la Riera dels Canyars). Recent studies of Cova Foradada point to the presence of several Châtelperronian elements, showing a rapid and complex Middle to Upper Palaeolithic transition (Morales et al., 2016). Unfortunately, the scarcity of human activity (i.e. no cut-marks, only 7 burnt bones and 14 lithics), is insufficient to determine the human activity at the Cova del Coll Verdaguer site, but what is clear is that this activity was unrelated to faunal accumulation, given the absence of cut-marks (Sanz and Daura, 2017).

The lithic assemblage of Cova del Coll Verdaguer is another good example in the Mediterranean basin of the Iberian Peninsula (Daura et al., 2015, 2013, 2010; Gusi et al., 2013; Rosell et al., 2010; Terradas and Rueda, 1998) of a Pleistocene palaeontological context with scarce human presence. At the site, the lithics correspond to sporadic, ephemeral visits by humans while the faunal assemblage, devoid of any anthropogenic damage, suggests the presence of carnivores as biological agents of the accumulation. Contexts of this kind, which some authors have defined as denning carnivores with sporadic human visits (Villa et al., 2004), are characterised by huge quantities of bone remains and few lithic implements. In some instances, the presence of the lithics have been attributed to accidental associations due to post-depositional processes (Villa and Soressi, 2000). Here, both the faunal and lithic records are quite different from those recovered at sites at which the residential function was dominant. The differences between the lithic assemblages found at several archaeological sites located in the same geographical area, including Cova del Rinoceront (Daura et al., 2015), are quite straightforward. Unlike Cova del Coll Verdaguer, small artefacts were dominant in Cova del Rinoceront and the degree of post-depositional damage was much higher. These characteristics suggest an accidental association for most of the Cova del Rinoceront lithics. In addition, the potential preferential selection of flakes with asymmetrical profiles, which is fairly clear in Cova del Coll Verdaguer, is totally absent in the Cova del Rinoceront assemblage. This careful selection of the artefacts supports the characterization of the Cova del Coll Verdaguer assemblage as a transported toolkit. These differences highlight the diversity of the formation processes responsible for these small assemblages.

The regional palaeoenvironmental and archaeological data obtained in the Garraf Massif could be indicative of the presence of several biomes between the plains with their large megafauna and the low mountain ranges with a relatively dense boreal forest, as indicated by the vegetation and faunal remains across the three main units. The abundance of carnivores in the cave and the paucity of biomass resources in the boreal forest probably account for the scarce presence of Neanderthals in this territory during the end of the Middle Palaeolithic.

6. Conclusion

The stratigraphic sequence of Cova del Coll Verdaguer provides a good archive for evaluating the terrestrial response to the rapid fluctuations at the beginning of MIS 3 in the NE of the Iberian Peninsula.

The multi-proxy palaeoenvironmental record, comprising 27 vegetal taxa identified by charcoal and pollen remains and 43 vertebrate and invertebrate faunal remains associated with a multi-method (U-Th, ESR, TL, AAR and 14C) chronological approach of 27 ages, provides a precise palaeoenvironmental reconstruction of a period between 34.2 and 56 ka BP in the Mediterranean coast of the Iberian Peninsula.

The palaeoenvironmental reconstruction reported in this study indicates that the floristic and faunal elements were initially related with open meadows at the base of the sequence. Subsequently, the arboreal component increases from the base to the top of the sequence signalling closed forest or woodland conditions. The results of this multi-proxy analysis are an important source of information for gaining a better understanding of the environmental conditions at the beginning of MIS 3 and, hence, of their relationship with the last Neanderthal populations on the peninsula.

The archaeological evidence from the cave is sporadic, signalling the varied range of complex behavioural patterns of Neanderthal populations in this territory, i.e. residential or more permanent occupations (Abric Romaní), short-term visits (Coll Verdaguer), and short-term occupations involving few Neanderthal individuals (Cova del Gegant). The archaeological sequence described herein depicts a more complex transition between the Middle and Upper Palaeolithic than has previously been reported in the region. Finally, the scarce presence of Neanderthal occupations is probably related to the poor sustainable environmental conditions of the boreal forest in the rocky Massif at the beginning of MIS 3.

Acknowledgments

This study is part of the output of a research project entitled: "*El Plistocè superior a la costa central catalana: paleoambients i ocupacions neandertals* (2014/100639- Servei d'Arqueologia i Paleontologia)", supported by projects 2014SGR-108, HAR2014-55131 and CGL2015-65387-C3-2-P (MINECO/FEDER). J. Daura holds a Ramon y Cajal contract (RYC-2015-17667) M. Sanz was supported by a Juan de la Cierva postdoctoral grant (FJCI-2014-21386). J. S. Carrión acknowledges funding from two projects – Séneca 19434/PI/14, and CGL-BOS 2015–68604, both directly related to this research project. L.J. Arnold was supported by Australian Research Council Future Fellowship grant FT130100195. We are especially grateful to Alejandro Gallardo (University of Barcelona) for his assistance in sorting the gastropods. Irradiations were performed in the Wadsworth Laboratories of the New York State Public Health Department, courtesy of Dr. David Lawrence, at the McMaster University, courtesy of Dr. Bonnie Blackwell. Sample ET32 was prepared by Dr. Blackwell and samples ET27 and ET33 were prepared by Justin Harris. Alice Pidruczny performed the NAA analyses at McMaster University. ESR experiments was supported by the National Science Foundation (Grant ILI-9151111), McMaster University and Williams College. Thanks to the Castelldefels City Council (La Guixera Laboratory) where the archaeological analyses were carried out.

References

Adam, W., 1960. Faune de Belgique. Mollusques. Tome I. Mollusques terrestres et dulcicoles. Institut Royal des Sciences Naturelles de Belgique, Bruxelles.

Aitken, M.J., 1998. An Introduction to Optical Dating: the Dating of Quaternary Sediments by the Use of Photon-stimulated Luminescence. Oxford University Press, Oxford.

Aitken, M.J., 1985. Thermoluminescence Dating. Academic Press, London.

Alejano, R., Montes, E.M., 2006. Aportaciones de la paleobotánica a la interpretación del área natural de *Pinus nigra* Arn. ssp. *salzmannii* en las Sierras Béticas (sureste de España). For. Syst. 15, 124–136.

Allué, E., Picornell-Gelabert, L., Daura, J., Sanz, M., 2017a. Reconstruction of the palaeoenvironment and anthropogenic activity from the Upper Pleistocene/Holocene anthracological records of the NE iberian peninsula (Barcelona, Spain). Quat. Int. https://doi.org/10.1016/j.quaint.2016.10.024.

Allué, E., Solé, A., Burguet-Coca, A., 2017b. Fuel exploitation among Neanderthals based on the anthracological record from Abric Romaní (Capellades, NE Spain).

Quat. Int. 431, 6–15. https://doi.org/10.1016/j.quaint.2015.12.046.
Álvarez-Lao, D.J., García, N., 2010. Chronological distribution of Pleistocene cold-adapted large mammal faunas in the Iberian Peninsula. Quat. Int. 212, 120–128. https://doi.org/10.1016/j.quaint.2009.02.029.
Álvarez-Lao, D.J., Méndez, M., 2016. Latitudinal gradients and indicator species in ungulate paleoassemblages during the MIS 3 in W Europe. Palaeogeogr. Palaeoclimatol. Palaeoecol. 449, 455–462. https://doi.org/10.1016/j.palaeo.2016.02.050.
Álvarez-Lao, D.J., Rivals, F., Sánchez-Hernández, C., Blasco, R., Rosell, J., 2017. Ungulates from teixoneres cave (Moià, Barcelona, Spain): presence of cold-adapted elements in NE iberia during the MIS 3. Palaeogeogr. Palaeoclimatol. Palaeoecol. 466, 287–302. https://doi.org/10.1016/j.palaeo.2016.11.040.
Andersen, K.K., Azuma, N., Barnola, J.-M., Bigler, M., Biscaye, P., Caillon, N., Chappellaz, J., Clausen, H.B., Dahl-Jensen, D., Fischer, H., Flückiger, J., Fritzsche, D., Fujii, Y., Goto-Azuma, K., Grønvold, K., Gundestrup, N.S., Hansson, M., Huber, C., Hvidberg, C.S., Johnsen, S.J., Jonsell, U., Jouzel, J., Kipfstuhl, S., Landais, A., Leuenberger, M., Lorrain, R., Masson-Delmotte, V., Miller, H., Motoyama, H., Narita, H., Popp, T., Rasmussen, S.O., Raynaud, D., Rothlisberger, R., Ruth, U., Samyn, D., Schwander, J., Shoji, H., Siggard-Andersen, M.-L., Steffensen, J.P., Stocker, T., Sveinbjörnsdóttir, A.E., Svensson, A., Takata, M., Tison, J.-L., Thorsteinsson, T., Watanabe, O., Wilhelms, F., White, J.W.C., 2004. High-resolution record of Northern Hemisphere climate extending into the last interglacial period. Nature 431, 147–151. https://doi.org/10.1038/nature02805.
Andrews, P., Turner, A., 1991. Life and death of the westbury bears. Ann. Zool. Fenn. 28, 139–149.
Arnold, L.J., Bailey, R.M., Tucker, G.E., 2007. Statistical treatment of fluvial dose distributions from southern Colorado arroyo deposits. Quat. Geochronol. 2, 162–167. https://doi.org/10.1016/j.quageo.2006.05.003.
Arnold, L.J., Demuro, M., Navazo, M., Benito-Calvo, A., Pérez-González, A., 2013. OSL dating of the Middle Palaeolithic Hotel California site, Sierra de Atapuerca, north-central Spain. Boreas 42, 285–305. https://doi.org/10.1111/j.1502-3885.2012.00262.x.
Arnold, L.J., Roberts, R.G., 2011. Paper I - optically stimulated luminescence (OSL) dating of perennially frozen deposits in north-central Siberia: OSL characteristics of quartz grains and methodological considerations regarding their suitability for dating. Boreas 40, 389–416. https://doi.org/10.1111/j.1502-3885.2011.00209.x.
Arnold, L.J., Roberts, R.G., 2009. Stochastic modelling of multi-grain equivalent dose (De) distributions: implications for OSL dating of sediment mixtures. Quat. Geochronol. 4, 204–230. https://doi.org/10.1016/j.quageo.2008.12.001.
Arnold, L.J., Roberts, R.G., Galbraith, R.F., DeLong, S.B., 2009. A revised burial dose estimation procedure for optical dating of youngand modern-age sediments. Quat. Geochronol. 4, 306–325. https://doi.org/10.1016/j.quageo.2009.02.017.
Arnold, L.J., Roberts, R.G., Macphee, R.D.E., Haile, J.S., Brock, F., Möller, P., Froese, D.G., Tikhonovo, A.N., Chivas, A.R., Gilbert, M.T.P., Willerslev, E., 2011. Paper II - dirt, dates and DNA: OSL and radiocarbon chronologies of perennially frozen sediments in Siberia, and their implications for sedimentary ancient DNA studies. Boreas 40, 417–445. https://doi.org/10.1111/j.1502-3885.2010.00181.x.
Auclair, M., Lamothe, M., Huot, S., 2003. Measurement of anomalous fading for feldspar IRSL using SAR. Radiat. Meas. 37, 487–492. https://doi.org/10.1016/S1350-4487(03)00018-0.
Badal, E., Villaverde, V., Zilhão, J., 2012. Middle Palaeolithic wood charcoal from three sites in south and West Iberia. Biogeographical implication. Saguntum Papeles del Lab. Arqueol. Valencia EXTRA 13, 13–24.
Bailey, G., 2007. Time perspectives, palimpsests and the archaeology of time. J. Anthropol. Archaeol. 26, 198–223. https://doi.org/10.1016/j.jaa.2006.08.002.
Bailey, G., Galanidou, N., 2009. Caves, palimpsests and dwelling spaces: examples from the Upper Palaeolithic of south-east Europe. World Archaeol. 41, 215–241. https://doi.org/10.1080/00438240902843733.
Ballesteros, D., Rodríguez-Rodríguez, L., González-Lemos, S., Giralt, S., Álvarez-Lao, D.J., Adrados, L., Jiménez-Sánchez, M., 2017. New evidence of sea-level lowstands and paleoenvironment during MIS 6 and 4 in the Cantabrian coastal karst: the Cobiheru cave (North Iberia). Earth Surf. Process. Landforms. https://doi.org/10.1002/esp.4115.
Bar-Matthews, M., Ayalon, A., Gilmour, M., Matthews, A., Hawkesworth, C.J., 2003. Sea–land oxygen isotopic relationships from planktonic foraminifera and speleothems in the Eastern Mediterranean region and their implication for paleorainfall during interglacial intervals. Geochim. Cosmochim. Acta 67, 3181–3199. https://doi.org/10.1016/S0016-7037(02)01031-1.
Bartrina, M.T., Cabrera, L., Jurado, M.J., Guimerà, J., Roca, E., 1992. Evolution of the central Catalan margin of the Valencia trough (western Mediterranean). Tectonophysics 203, 219–247. https://doi.org/10.1016/0040-1951(92)90225-U.
Bech, M., 1990. Fauna malacològica de Catalunya: mol·luscs terrestres i d'aigua dolça. Treballs la Inst. Catalana d'Història Nat. 12, 1–229.
Bennett, K.D., 2000. Psimpoll and pscomb: computer programs for data plotting and analysis. [WWW Document]. Psimpoll and pscomb: computer programs for data plotting and analysis. http://www.kv.geo.uu.se/software.html.
Berger, G.W., Pérez-González, A., Carbonell, E., Arsuaga, J.L., Bermúdez de Castro, J.-M., Ku, T.-L., 2008. Luminescence chronology of cave sediments at the Atapuerca paleoanthropological site, Spain. J. Hum. Evol. 55, 300–311. https://doi.org/10.1016/j.jhevol.2008.02.012.
Beyries, S., Boëda, E., 1983. Etude technologique et traces d'utilisation des 'éclats débordants' de Corbehem (Pas-de-Calais). Bull. la Société Préhistorique Française 80, 275–279.
Bischoff, J.L., Fitzpatrick, J.A., 1991. U-series dating of impure carbonates: an isochron technique using total-sample dissolution. Geochim. Cosmochim. Acta 55, 543–554. https://doi.org/10.1016/0016-7037(91)90011-S.
Bischoff, J.L., Julià, R., Mora, R., 1988. Uranium-series dating of the mousterian occupation at Abric-Romani, Spain. Nature 332, 68–70.
Blackwell, B.A.B., Montoya, A., Blickstein, J.I.B., Skinner, A.R., Pappu, S., Gunnell, Y., Taieb, M., Kumar, A., Lundberg, J.A., 2007. ESR analyses for teeth from the open-air site at Attirampakkam, India: clues to complex U uptake and paleoenvironmental change. Radiat. Meas. 42, 1243–1249. https://doi.org/10.1016/j.radmeas.2007.05.040.
Blackwell, B.A.B., Skinner, A.R., Blickstein, J.I.B., Montoya, A.C., Florentin, J.A., Baboumian, S.M., Ahmed, I.J., Deely, A.E., 2016. ESR in the 21st century: from buried valleys and deserts to the deep ocean and tectonic uplift. Earth-Science Rev. 158, 125–159. https://doi.org/10.1016/j.earscirev.2016.01.001.
Bogatell, S., 1930. Parlant de vidre. La Veu de Catalunya. Diari Català d'Avisos. Not. i Anunc. 40, 2.
Borredà, V., Martínez-Ortí, A., Nicolau, J., 2010. Guia de camp dels mol·luscs d'Andorra. Monografies del CENMA.
Brock, F., Thomas Higham, B., Peter Ditchfield, B., Christopher Bronk Ramsey, B., 2010. Current pretreatment methods for AMS radiocarbon dating at the Oxford radiocarbon accelerator unit (ORAU). Radiocarbon 52, 103–112. https://doi.org/10.1017/S0033822200045069.
Bronk Ramsey, C., 2009. Bayesian analysis of radiocarbon dates. Radiocarbon 51, 337–360. https://doi.org/10.1017/S0033822200033865.
Brugal, J.-P., Fosse, P., Guadelli, J.-L., 1997. Comparative study of bone assemblages made by recent and Pleistocene Hyenids. In: Proceedings of the 1993 Bone Modification Conference, Hot Springs, South Dakota. Archeology Laboratory, Augustana College. Occasional Publication, Sioux Falls, pp. 158–187.
Burjachs, F., López-García, J.M., Allué, E., Blain, H.-A., Rivals, F., Bennàsar, M., Expósito, I., 2012. Palaeoecology of Neanderthals during dansgaard–oeschger cycles in northeastern iberia (Abric Romaní): from regional to global scale. Quat. Int. 247, 26–37. https://doi.org/10.1016/j.quaint.2011.01.035.
Cacho, I., Grimalt, J.O., Pelejero, C., Canals, M., Sierro, F.J., Flores, J.A., Shackleton, N., 1999. Dansgaard-oeschger and Heinrich event imprints in Alboran sea paleotemperatures. Paleoceanography 14, 698–705. https://doi.org/10.1029/1999PA900044.
Cadevall, J., Orozco, A., 2016. Caracoles y babosas de la Península Ibérica y Baleares. Nuevas Guías de campo Omega. Omega.
Carrión, J., 2004. Two pollen deep sea cores to frame adaptive evolutionary change for humans. A comment on 'Neandertal extinction and the millennial scale climatic variability of OIS 3' by F. dErrico & M.F. Sánchez Goñi. Quat. Sci. Rev. 23, 1217–1224.
Carrión, J.S., 2002. Patterns and processes of Late Quaternary environmental change in a montane region of southwestern Europe. Quat. Sci. Rev. 21, 2047–2066. https://doi.org/10.1016/S0277-3791(02)00010-0.
Carrión, J.S., Finlayson, C., Fernández, S., Finlayson, G., Allué, E., López-Sáez, J.A., López-García, P., Gil-Romera, G., Bailey, G., González-Sampériz, P., 2008. A coastal reservoir of biodiversity for Upper Pleistocene human populations: palaeoecological investigations in Gorham's Cave (Gibraltar) in the context of the Iberian Peninsula. Quat. Sci. Rev. 27, 2118–2135. https://doi.org/10.1016/j.quascirev.2008.08.016.
Carrión, J.S., Leroy, S., 2010. Iberian floras through time: land of diversity and survival. Rev. Palaeobot. Palynology 162, 227–230.
Chabal, L., Fabre, L., Terral, J.F., Théry-Parisot, I., 1999. In: Ferdière, A., La Botanique (Eds.), L'anthracologie. Errance, Paris, pp. 43–104.
Cheng, H., Edwards, R., Hoff, J., Gallup, C., Richards, D., Asmerom, Y., 2000. The half-lives of uranium-234 and thorium-230. Chem. Geol. 169, 17–33.
Crégut-Bonnoure, E., 2005. Nouvelles données paléogéographiques et chronologiques sur les Caprinae (Mammalia, Bovidae) du Pléistocène moyen et supérieur d'Europe. Munibe. Antropologia-arkeologia 57, 205–219.
d'Errico, F., Sánchez Goñi, M.F., 2003. Neandertal extinction and the millennial scale climatic variability of OIS 3. Quat. Sci. Rev. 22, 769–788. https://doi.org/10.1016/S0277-3791(03)00009-X.
Daura, J., 2008. Caracterització arqueològica i paleontològica dels jaciments pliscotens: massís del Garraf-Ordal i curs baix del riu Llobregat. Ph.D. thesis. Universitat de Barcelona.
Daura, J., Sanz, M., Fornós, J.J., Asensio, A., Julià, A.R., 2014. Karst evolution of the Garraf Massif (Barcelona, Spain): doline formation, chronology and archaeopalaeontological archives. J. Cave Karst Stud. 76, 69–87. https://doi.org/10.4311/2011ES0254.
Daura, J., Sanz, M., García, N., Allué, E., Vaquero, M., Fierro, E., Carrión, J.S., López-García, J.M., Blain, H.A., Sánchez-Marco, A., Valls, C., Albert, R.M., Fornós, J.J., Julià, R., Fullola, J.M., Zilhão, J., 2013. Terrasses de la Riera dels Canyars (Gavà, Barcelona): the landscape of Heinrich Stadial 4 north of the 'Ebro frontier' and implications for modern human dispersal into Iberia. Quat. Sci. Rev. 60, 26–48. https://doi.org/10.1016/j.quascirev.2012.10.042.
Daura, J., Sanz, M., Julià, R., García-Fernández, D., Fornós, J.J., Vaquero, M., Allué, E., López-García, J.M., Blain, H.A., Ortiz, J.E., Torres, T., Albert, R.M., Rodríguez-Cintas, À., Sánchez-Marco, A., Cerdeño, E., Skinner, A.R., Asmeron, Y., Polyak, V.J., Garcés, M., Arnold, L.J., Demuro, M., Pike, A.W.G., Euba, I., Rodríguez, R.F., Yagüe, A.S., Villaescusa, L., Gómez, S., Rubio, A., Pedro, M., Fullola, J.M., Zilhão, J., 2015. Cova del Rinoceront (Castelldefels, Barcelona): a terrestrial record for the Last Interglacial period (MIS 5) in the Mediterranean coast of the Iberian Peninsula. Quat. Sci. Rev. 114, 203–227. https://doi.org/10.1016/j.quascirev.2015.02.014.

Daura, J., Sanz, M., Pike, A.W.G., Subirà, M.E., Fornós, J.J., Fullola, J.M., Julià, R., Zilhão, J., 2010. Stratigraphic context and direct dating of the Neandertal mandible from Cova del Gegant (Sitges, Barcelona). J. Hum. Evol. 59, 109–122. https://doi.org/10.1016/j.jhevol.2010.04.009.

Demuro, M., Arnold, L.J., Froese, D.G., Roberts, R.G., 2013. OSL dating of loess deposits bracketing Sheep Creek tephra beds, northwest Canada: dim and problematic single-grain OSL characteristics and their effect on multi-grain age estimates. Quat. Geochronol. 15, 67–87. https://doi.org/10.1016/j.quageo.2012.11.003.

Demuro, M., Arnold, L.J., Parés, J.M., Sala, R., 2015. Extended-range luminescence chronologies suggest potentially complex bone accumulation histories at the Early-to-Middle Pleistocene palaeontological site of Huéscar-1 (Guadix-Baza basin, Spain). Quat. Int. 389, 191–212. https://doi.org/10.1016/j.quaint.2014.08.035.

Domínguez-Villar, D., Carrasco, R.M., Pedraza, J., Cheng, H., Edwards, R.L., Willenbring, J.K., 2013. Early maximum extent of paleoglaciers from Mediterranean mountains during the last glaciation. Sci. Rep. 3, 2034. https://doi.org/10.1038/srep02034.

Fick, O.K.W., 1974. Vergleichend Morphologische Untersuchungen an Einzelknochen Europäischer Taubenarten. Institut für Paläoanatomie, Domes-¬tikationsforschung und Geschich¬te der Tiermedizin der Universität München, Munich.

Finlayson, C., 2004. Neanderthals and Modern Humans: an Ecological and Evolutionary Perspective. Cambridge University Press.

Finlayson, C., Carrión, J.S., 2007. Rapid ecological turnover and its impact on Neanderthal and other human populations. Trends Ecol. Evol. 22, 213–222.

Finlayson, C., Giles Pacheco, F., Rodríguez-Vidal, J., Fa, D.A., María Gutierrez López, J., Santiago Pérez, A., Finlayson, G., Allue, E., Baena Preysler, J., Cáceres, I., Carrión, J.S., Fernández Jalvo, Y., Gleed-Owen, C.P., Jimenez Espejo, F.J., López, P., Antonio López Sáez, J., Antonio Riquelme Cantal, J., Sánchez Marco, A., Giles Guzman, F., Brown, K., Fuentes, N., Valarino, C.A., Villalpando, A., Stringer, C.B., Martinez Ruiz, F., Sakamoto, T., 2006. Late survival of Neanderthals at the southernmost extreme of Europe. Nature 443, 850–853. https://doi.org/10.1038/nature05195.

Fletcher, W.J., Sánchez Goñi, M.F., 2008. Orbital- and sub-orbital-scale climate impacts on vegetation of the western Mediterranean basin over the last 48,000 yr. Quat. Res. 70, 451–464. https://doi.org/10.1016/j.yqres.2008.07.002.

Fletcher, W.J., Sánchez Goñi, M.F., Allen, J.R.M., Cheddadi, R., Combourieu-Nebout, N., Huntley, B., Lawson, I., Londeix, L., Magri, D., Margari, V., Müller, U.C., Naughton, F., Novenko, E., Roucoux, K., Tzedakis, P.C., 2010. Millennial-scale variability during the last glacial in vegetation records from Europe. Quat. Sci. Rev. 29, 2839–2864. https://doi.org/10.1016/j.quascirev.2009.11.015.

Font-Tullot, I., 2000. Climatología de España y Portugal. Ediciones Universidad de Salamanca, Salamanca.

Furió, M., 2007. Los Insectívoros (Soricomorpha, Erinaceomorpha, Mammalia) del Neógeno superior del levante Ibérico. Phd Thesis. Departament de Geología, Universitat Autónoma de Barcelona, Barcelona.

Gabucio, M.J., Caceres, I., Rodriguez-Hidalgo, A., Rosell, J., Saladie, P., 2014. A wildcat (Felis silvestris) butchered by Neanderthals in level O of the Abric Romani site (capellades, Barcelona, Spain). Quat. Int. 326, 307–318.

García García, N., Feranec, R.S., Arsuaga, J.L., Bermúdez de Castro, J.M., Carbonell, E., 2009. Isotopic analysis of the ecology of herbivores and carnivores from the Middle Pleistocene deposits of the Sierra De Atapuerca, northern Spain. J. Archaeol. Sci. 36, 1142–1151. https://doi.org/10.1016/j.jas.2008.12.018.

Gebert, C., Verheyden-Tixier, H., 2008. Variations of diet composition of red deer (*Cervus elaphus* L.) in Europe. Mammal. Rev. 31, 189–201. https://doi.org/10.1111/j.1365-2907.2001.00090.x.

Gómez-Olivencia, A., Arceredillo, D., Álvarez-Lao, D.J., Garate, D., San Pedro, Z., Castaños, P., Rios-Garaizar, J., 2014. New evidence for the presence of reindeer (*Rangifer tarandus*) on the Iberian Peninsula in the Pleistocene: an archaeopalaeontological and chronological reassessment. Boreas 43, 286–308. https://doi.org/10.1111/bor.12037.

González-Sampériz, P., Leroy, S.A.G., Carrión, J.S., Fernández, S., García-Antón, M., Gil-García, M.J., Uzquiano, P., Valero-Garcés, B., Figueiral, I., 2010. Steppes, savannahs, forests and phytodiversity reservoirs during the Pleistocene in the Iberian Peninsula. Rev. Palaeobot. Palynology 162, 427–457. https://doi.org/10.1016/j.revpalbo.2010.03.009.

Grün, R., McDermott, F., 1994. Open system modelling for U-series and ESR dating of teeth. Quat. Sci. Rev. 13, 121–125. https://doi.org/10.1016/0277-3791(94)90037-X.

Guimerà, A., 1988. Estudi estructural de l'enllaç entre la Serralada Ibèrica i la Serralada Costanera Catalana. Ph.D. thesis. Universitat de Barcelona.

Gusi, F., Olària, C., Ollé, A., Saladié, P., Vallverdú, J., Cáceres, I., Van Der Made, J., Expósito, I., Burjachs, F., López-Polín, L., Lorenzo, C., Bennàsar, M., Salazar-García, D.C., Carbonell, E., 2013. La Cova de Dalt del Tossal de la Font (Vilafamés, Castellón): conclusiones preliminares de las intervenciones arqueológicas (1982-1987/2004-2012). Quad. prehistòria Arqueol. Castelló 31, 17–37.

Haas, F., 1929. Fauna malacológica terrestre y de agua dulce de Cataluña. Trab. del Mus. Ciencias Nat. Barc. 13, 1–491.

Harrison, S.P., Sanchez Goñi, M.F., 2010. Global patterns of vegetation response to millennial-scale variability and rapid climate change during the last glacial period. Quat. Sci. Rev. 29, 2957–2980. https://doi.org/10.1016/j.quascirev.2010.07.016.

Heinz, C., Barbaza, M., 1998. Environmental changes during the Late Glacial and Post-Glacial in the central Pyrenees (France): new charcoal analysis and archaeological data. Rev. Palaeobot. Palynology 104, 1–17. https://doi.org/10.1016/S0034-6667(98)00050-5.

Higham, T., Brock, F., Peresani, M., Broglio, A., Wood, R., Douka, K., 2009. Problems with radiocarbon dating the middle to upper palaeolithic transition in Italy. Quat. Sci. Rev. 28, 1257–1267. https://doi.org/10.1016/j.quascirev.2008.12.018.

Hodge, E.J., Richards, D.A., Smart, P.L., Andreo, B., Hoffmann, D.L., Mattey, D.P., González-Ramón, A., 2008. Effective precipitation in southern Spain (~266 to 46 ka) based on a speleothem stable carbon isotope record. Quat. Res. 69, 447–457. https://doi.org/10.1016/j.yqres.2008.02.013.

Hoffmann, D.L., Pike, A.W.G., García-Diez, M., Pettitt, P.B., Zilhão, J., 2016. Methods for U-series dating of CaCO3 crusts associated with Palaeolithic cave art and application to Iberian sites. Quat. Geochronol. 36, 104–119.

Hoffmann, D.L., Prytulak, J., Richards, D.A., Elliott, T., Coath, C.D., Smart, P.L., Scholz, D., 2007. Procedures for accurate U and Th isotope measurements by high precision MC-ICPMS. Int. J. Mass Spectrom. 264, 97–109.

Hoffmann, D.L., Utrilla, P., Bea, M., Pike, A.W.G., García-Diez, M., Zilhão, J., Domingo, R., 2017. U-series dating of Palaeolithic rock art at Fuente del Trucho (Aragón, Spain). Quat. Int. 432, 50–58. https://doi.org/10.1016/j.quaint.2015.11.111.

Holden, N.E., 1990. Total half-lives for selected nuclides. Pure Appl. Chem. 62, 941–958.

Huntley, D.J., Lamothe, M., 2001. Ubiquity of anomalous fading in K-feldspars and the measurement and correction for it in optical dating. Can. J. Earth Sci. 38, 1093–1106. https://doi.org/10.1139/e01-013.

Ivanovich, M., Harmon, R.S., 1992. Uranium-series Disequilibrium: Application to Earth, Marine and Environmental Sciences, second ed. Clarendon Press, Oxford.

Jaffey, A.H., Flynn, K.F., Glendenin, L.E., Bentley, W.C., Essling, A.M., 1971. Precision measurement of half-lives and specific activities of 235U and 238U. Phys. Rev. C 4, 1889.

Jennings, R.P., Giles Pacheco, F., Barton, R.N.E., Collcutt, S.N., Gale, R., Gleed-Owen, C.P., Gutiérrez López, J.M., Higham, T.F.G., Parker, A., Price, C., Rhodes, E., Santiago Pérez, A., Schwenninger, J.L., Turner, E., 2009. New dates and palaeoenvironmental evidence for the Middle to Upper Palaeolithic occupation of Higueral de Valleja Cave, southern Spain. Quat. Sci. Rev. 28, 830–839. https://doi.org/10.1016/j.quascirev.2008.11.014.

Kaufman, D.S., 2006. Temperature sensitivity of aspartic and glutamic acid racemization in the foraminifera Pulleniatina. Quat. Geochronol. 1, 188–207. https://doi.org/10.1016/j.quageo.2006.06.008.

Kaufman, D.S., 2000. Amino acid racemization in ostracodes. In: Goodfriend, G.A., Collins, M.J., Fogel, M.L., Macko, S.A., Wehmiller, J.F. (Eds.), Perspectives in Amino Acids and Protein Geochemistry. Oxford University Press, New York, pp. 145–160.

Kaufman, D.S., Manley, W.F., 1998. A new procedure for determining DL amino acid ratios in fossils using reverse phase liquid chromatography. Quat. Sci. Rev. 17, 987–1000. https://doi.org/10.1016/S0277-3791(97)00086-3.

Lisiecki, L.E., Raymo, M.E., 2005. A Pliocene-Pleistocene stack of 57 globally distributed benthic δ 18 O records. Paleoceanography 20. https://doi.org/10.1029/2004PA001071 n/a–n/a.

Lister, A.M., 1996. The morphological distinction between bones and teeth of fallow deer (*Dama dama*) and red deer (*Cervus elaphus*). Int. J. Osteoarchaeol. 6, 119–143. https://doi.org/10.1002/(SICI)1099-1212(199603)6:2<119::AID-OA265>3.0.CO;2–8.

Llopis Lladó, N., 1941. Morfología e hidrología subterránea de la parte oriental del macizo cárstico de Garraf (Barcelona). Estud. Geográficos 2, 413–466.

Locard, A., 1894. Les coquilles terrestre de France. Librairie J.-B. Baillière et Fils, Paris.

López García, J.M., Berto, C., Luzi, E., Dalla Valle, C., Bañuls Cardona, S., Sala, B., 2015. The genus Iberomys (chaline, 1972) (rodentia, arvicolinae, mammalia) in the Pleistocene of Italy. Italian J. Geosciences 134, 162–169. https://doi.org/10.3301/IJG.2014.48.

López-García, J.M., Blain, H.-A., Cuenca-Bescós, G., Ruiz-Zapata, M.B., Dorado-Valiño, M., Gil-García, M.J., Valdeolmillos, A., Ortega, A.I., Carretero, J.M., Arsuaga, J.L., de Castro, J.M.B., Carbonell, E., 2010. Palaeoenvironmental and palaeoclimatic reconstruction of the Latest Pleistocene of El Portalón Site, Sierra de Atapuerca, northwestern Spain. Palaeogeogr. Palaeoclimatol. Palaeoecol. 292, 453–464. https://doi.org/10.1016/j.palaeo.2010.04.006.

Maroto, J., Arrizabalaga, Á., Baena, J., Baquedano, E., Jordá, J., Julià, R., Montes, R., Van Der Plicht, J., Rasines, P., Wood, R., 2012. Current issues in late middle palaeolithic chronology: new assessments from northern Iberia. Quat. Int. 247, 15–25. https://doi.org/10.1016/j.quaint.2011.07.007.

Martrat, B., 2004. Abrupt temperature changes in the western mediterranean over the past 250,000 years. Science 306, 1762–1765. https://doi.org/10.1126/science.1101706.

Mazon, L.I., de Pancorbo, M.A.M., Vicario, A., Aguirre, A.I., Estomba, A., Lostao, C.M., 1987. Distribution of *Cepaea nemoralis* according to climatic regions in Spain. Heredity 58, 145–154. https://doi.org/10.1038/hdy.1987.19.

Morales, J.I., Tejero, J.-M., Cebrià, A., Rodríguez-Hidalgo, A., Soto1, M., Vallverdú1, J., Saladié, P., Allué1, E., García-Agudo, G., Fernández-Marchena, J., López-García1, J.M., Fullola, J.M., 2016. A southern snapshot of the middle-to-upper paleolithic transition: Foradada cave (Calafell, Tarragona, Spain. In: 6th Annual Meeting of the European Society for the Study of Human Evolution. Proceedings of the European Society for the study of Human Evolution, 5, p. 170.

Moreno, A., Stoll, H., Jiménez-Sánchez, M., Cacho, I., Valero-Garcés, B., Ito, E., Edwards, R.L., 2010. A speleothem record of glacial (25–11.6kyr BP) rapid climatic changes from northern Iberian Peninsula. Glob. Planet. Change 71, 218–231. https://doi.org/10.1016/j.gloplacha.2009.10.002.

Nambi, K.S.V., Aitken, M.J., 1986. Annual dose conversion factors for TL and ESR dating. Archaeometry 28 (2), 202–205. https://doi.org/10.1111/j.1475-4754.1986.tb00388.x.
Porat, N., Schwarcz, H.P., 1994. ESR dating of tooth enamel: a universal growth curve. In: Corrucini, R.S., Ciochon, R.L. (Eds.), Integrative Paths to the Past, Paleoanthropological Advances in Honor of F. Clark Howell. Prentice Hall, Englewood, New Jersey, pp. 521–530.
Rabineau, M., Berné, S., Olivet, J.-L., Aslanian, D., Guillocheau, F., Joseph, P., 2006. Paleo sea levels reconsidered from direct observation of paleoshoreline position during Glacial Maxima (for the last 500,000 yr). Earth Planet. Sci. Lett. https://doi.org/10.1016/j.epsl.2006.09.033.
Rasmussen, S.O., Seierstad, I.K., Andersen, K.K., Bigler, M., Dahl-Jensen, D., Johnsen, S.J., 2008. Synchronization of the NGRIP, GRIP, and GISP2 ice cores across MIS 2 and palaeoclimatic implications. Quat. Sci. Rev. 27, 18–28. https://doi.org/10.1016/j.quascirev.2007.01.016.
Reimer, P., 2013. IntCal13 and Marine13 radiocarbon age calibration curves 0–50,000 Years cal BP. Radiocarbon 55, 1869–1887. https://doi.org/10.2458/azu_js_rc.55.16947.
Reitz, E.J., Wing, E.S., 2008. Zooarchaeology.
Richards, M.P., Pacher, M., Stiller, M., Quiles, J., Hofreiter, M., Constantin, S., Zilhao, J., Trinkaus, E., 2008. Isotopic evidence for omnivory among European cave bears: late Pleistocene Ursus spelaeus from the Pestera cu Oase, Romania. Proc. Natl. Acad. Sci. 105, 600–604. https://doi.org/10.1073/pnas.0711063105.
Rink, W., 1997. Electron spin resonance (ESR) dating and ESR applications in quaternary science and archaeometry. Radiat. Meas. 27, 975–1025. https://doi.org/10.1016/S1350-4487(97)00219-9.
Rivas-Martinez, S., Rivas-Saenz, S., 1996. Worldwide Bioclimatic Classification System [WWW Document]. http://www.globalbioclimatics.org.
Roiron, P., Chabal, L., Figueiral, I., Terral, J.-F., Ali, A.A., 2013. Palaeobiogeography of Pinus nigra Arn. subsp. salzmannii (Dunal) Franco in the north-western Mediterranean Basin: a review based on macroremains. Rev. Palaeobot. Palynology 194, 1–11.
Ros, M., 1987. L'anàlisi antracològica de la Cova de l'Arbreda (Serinyà, Gironès). Cypsela 6, 67–71.
Rosell, J., Blasco, R., Rivals, F., Chacón, M.G., Menéndez, L., Morales, J.I., Rodríguez-Hidalgo, A., Cebrià, A., Carbonell, E., Serrat, D., 2010. A stop along the way: the role of Neanderthal groups at level III of Teixoneres cave (Moià, Barcelona, Spain). Quaternaire 21, 139–154.
Rosenbauer, R.J., 1991. UDATE1: a computer program for the calculation of uranium-series isotopic ages. Comput. Geosciences 17, 45–75. https://doi.org/10.1016/0098-3004(91)90079-S.
Ruiz, A., Cárcaba, A., Porras, A., Arrébola, J.R., 2006. Caracoles terrestres de Andalucía. Guía y manual de identificación. Fundación Gyapaetus, Junta de Andalucia.
Sala, N., Arsuaga, J.L., 2013. Taphonomic studies with wild brown bears (*Ursus arctos*) in the mountains of northern Spain. J. Archaeol. Sci. 40, 1389–1396. https://doi.org/10.1016/j.jas.2012.10.018.
Sánchez Goñi, M., Cacho, I., Turon, J., Guiot, J., Sierro, F., Peypouquet, J., Grimalt, J., Shackleton, N., 2002. Synchroneity between marine and terrestrial responses to millennial scale climatic variability during the last glacial period in the Mediterranean region. Clim. Dyn. 19, 95–105. https://doi.org/10.1007/s00382-001-0212-x.
Sanchez Goñi, M.F., Harrison, S.P., 2010. Millennial-scale climate variability and vegetation changes during the Last Glacial: concepts and terminology. Quat. Sci. Rev. 29, 2823–2827. https://doi.org/10.1016/j.quascirev.2009.11.014.
Sánchez Goñi, M.F., Landais, A., Fletcher, W.J., Naughton, F., Desprat, S., Duprat, J., 2008. Contrasting impacts of Dansgaard–Oeschger events over a western European latitudinal transect modulated by orbital parameters. Quat. Sci. Rev. 27, 1136–1151. https://doi.org/10.1016/j.quascirev.2008.03.003.
Sánchez Marco, A., 2004. Avian zoogeographical patterns during the Quaternary in the Mediterranean region and paleoclimatic interpretation. Ardeola 51, 91–132.
Sánchez-Marco, A., 1996. Aves fósiles del Pleistoceno Ibérico: rasgos climáticos, ecológicos y zoo-geográficos. Ardeola 43, 207–219.
Sanz, M., 2013. Patrons d'acumulació de restes de fauna del Plistocè superior al nord-est peninsular (àrea del Massís del Garraf-Ordal). Ph.D. thesis. Universitat de Barcelona.
Sanz, M., Daura, J., 2017. Carnivore involvement in bone assemblages based on taphonomic and zooarchaeological analyses of Cova del Coll Verdaguer site (Barcelona, Iberian Peninsula). Hist. Biol. XX–XXX. https://doi.org/10.1080/08912963.2017.1351561 (in press).
Sanz, M., Daura, J., Égüez, N., Brugal, J.-P., 2016. Not only hyenids: a multi-scale analysis of Upper Pleistocene carnivore coprolites in Cova del Coll Verdaguer (NE Iberian Peninsula). Palaeogeogr. Palaeoclimatol. Palaeoecol. 443, 249–262. https://doi.org/10.1016/j.palaeo.2015.11.047.
Schwarcz, H.P., 1985. ESR studies of tooth enamel (1982). Nucl. Tracks Radiat. Meas. 10, 865–867. https://doi.org/10.1016/0735-245X(85)90101-2.
Schweingruber, F.H., 1990. Anatomie europäischer Hölzer ein Atlas zur Bestimmung europäischer Baum-, Strauch- und Zwergstrauchhölzer. Anatomy of European woods an atlas for the identification of European trees shrubs and dwarf shrubs. Verlag Paul Haupt, Stuttgart.
Sepulchre, P., Ramstein, G., Kageyama, M., Vanhaeren, M., Krinner, G., Sánchez-Goñi, M.-F., D'Errico, F., 2007. H4 abrupt event and late Neanderthal presence in Iberia. Earth Planet. Sci. Lett. 258, 283–292. https://doi.org/10.1016/j.epsl.2007.03.041.
Skinner, A.R., 2014. Electron spin resonance (ESR) dating: general principles. In: Rink, W.J., Thmpson, J. (Eds.), Encyclopedia of Scienfific Dating Methods. Springer, Heidelberg, pp. 1–17.
Skinner, A.R., Blackwell, B.A.B., Chasteen, N.D., Shao, J., Min, S.S., 2000. Improvements in dating tooth enamel by ESR. Appl. Radiat. Isotopes 52, 1337–1344. https://doi.org/10.1016/S0969-8043(00)00092-0.
Spooner, N.A., 1994. On the optical dating signal from quartz. Radiat. Meas. 23, 593–600. https://doi.org/10.1016/1350-4487(94)90105-8.
Stiner, M.C., 2005. The Faunas of Hayonim Cave, Israel: a 200,000-year Record of Paleolithic Diet, Demography, and Society. Harvard University Press, USA.
Stoll, H.M., Moreno, A., Mendez-Vicente, A., Gonzalez-Lemos, S., Jimenez-Sanchez, M., Dominguez-Cuesta, M.J., Edwards, R.L., Cheng, H., Wang, X., 2013. Paleoclimate and growth rates of speleothems in the northwestern Iberian Peninsula over the last two glacial cycles. Quat. Res. 80, 284–290. https://doi.org/10.1016/j.yqres.2013.05.002.
Talamo, S., Blasco, R., Rivals, F., Picin, A., Gema Chacón, M., Iriarte, E., Manuel López-García, J., Blain, H.-A., Arilla, M., Rufà, A., Sánchez-Hernández, C., Andrés, M., Camarós, E., Ballesteros, A., Cebrià, A., Rosell, J., Hublin, J.-J., 2016. The radiocarbon approach to Neanderthals in a carnivore den site: a well-defined chronology for Teixoneres cave (Moià, Barcelona, Spain). Radiocarbon 1–19. https://doi.org/10.1017/RDC.2015.19.
Terradas, X., Rueda, J.M., 1998. Grotte 120: un exemple des activités de subsistance au Paléolithique moyen dans les Pyrénées orientales. In: Brugal, J.-P., Meignen, L., Patou-Mathis, M. (Eds.), Économie Préhistorique: Les Comportements de Subsistance Au Paléolithique, pp. 349–362.
Torres, T., Llamas, J.F., Canoira, L., García-Alonso, P., García-Cortés, A., Mansilla, H., 1997. Amino acid chronology of the lower Pleistocene deposits of venta micena (Orce, Granada, Andalusia, Spain). Org. Geochem. 26, 85–97. https://doi.org/10.1016/S0146-6380(96)00131-3.
Uzquiano, P., 2008. Domestic fires and vegetation cover among Neanderthalians and anatomically modern human groups (> 53 to 30 kyrs BP) in the cantabrian region (Cantabria, northern Spain). In: Fiorentino, G., Magri, D. (Eds.), Charcoal from the Past. Cultural and Palaeoenvironmental Implications, London, pp. 273–285.
Uzquiano, P., Yravedra, J., Zapata, B.R., Gil Garcia, M.J., Sesé, C., Baena, J., 2012. Human behaviour and adaptations to MIS 3 environmental trends (>53–30 ka BP) at Esquilleu cave (Cantabria, northern Spain). Quat. Int. 252, 82–89. https://doi.org/10.1016/j.quaint.2011.07.023.
Vaquero, M., Chacón, M.G., Cuartero, F., García-Antón, M.D., Gómez de Soler, B., Martínez, K., 2012. The lithic assemblage of level J. In: Carbonell, E. (Ed.), High Resolution Archaeology and Neanderthal Behavior. Time and Space in Level J of Abric Romaní (Capellades; Spain). Springer, Netherlands, pp. 189–311. https://doi.org/10.1007/978-94-007-3922-2_7.
Vernet, J.-L., 2006. History of the Pinus sylvestris and Pinus nigra ssp. salzmanni forest in the Sub-Mediterranean mountains (Grands Causses, Saint-Guilhem-le-Désert, southern Massif Central, France) based on charcoal from limestone and dolomitic deposits. Veg. Hist. Archaeobotany 16, 23–42. https://doi.org/10.1007/s00334-005-0032-8.
Villa, P., Castel, J.-C., Beauval, C., Bourdillat, V., Goldberg, P., 2004. Human and carnivore sites in the European Middle and Upper Paleolithic: similarities and differences in bone modification and fragmentation. In: Brugal, J.-P., Fosse, P. (Eds.), Actes du XIV Congrès UISPP 'Hommes & Carnivores au Paléolithique', Liège 2001, vol. 23. Revue de Paléobiologie, pp. 705–730.
Villa, P., Sánchez Goñi, M.F., Bescós, G.C., Grün, R., Ajas, A., García Pimienta, J.C., Lees, W., 2010. The archaeology and paleoenvironment of an Upper Pleistocene hyena den: an integrated approach. J. Archaeol. Sci. 37, 919–935. https://doi.org/10.1016/j.jas.2009.11.025.
Villa, P., Soressi, M., 2000. Stone tools in carnivore sites: the case of bois roche. J. Anthropol. Res. 56, 187–215. https://doi.org/10.1086/jar.56.2.3631362.
Wainer, K., Genty, D., Blamart, D., Daëron, M., Bar-Matthews, M., Vonhof, H., Dublyansky, Y., Pons-Branchu, E., Thomas, L., van Calsteren, P., Quinif, Y., Caillon, N., 2011. Speleothem record of the last 180 ka in Villars cave (SW France): investigation of a large δ18O shift between MIS6 and MIS5. Quat. Sci. Rev. 30, 130–146. https://doi.org/10.1016/j.quascirev.2010.07.004.
Welter-Schultes, F., 2012. European non-marine molluscs, a guide for species identification. Planet Poster Editions, Göttingen.
Wintle, A.G., 1973. Anomalous fading of thermo-luminescence in mineral samples. Nature 245, 143–144. https://doi.org/10.1038/245143a0.
Wood, R.E., Arrizabalaga, A., Camps, M., Fallon, S., Iriarte-Chiapusso, M.-J., Jones, R., Maroto, J., de la Rasilla, M., Santamaría, D., Soler, J., Soler, N., Villaluenga, A., Higham, T.F.G., 2014. The chronology of the earliest upper palaeolithic in northern Iberia: new insights from L'Arbreda, Labeko Koba and La Viña. J. Hum. Evol. 69, 91–109. https://doi.org/10.1016/j.jhevol.2013.12.017.
Wood, R.E., Barroso-Ruíz, C., Caparrós, M., Jordá Pardo, J.F., Galván Santos, B., Higham, T.F.G., 2013. Radiocarbon dating casts doubt on the late chronology of the Middle to Upper Palaeolithic transition in southern Iberia. Proc. Natl. Acad. Sci. U. S. A. 110, 2781–2786. https://doi.org/10.1073/pnas.1207656110.
Zilhão, J., 2009. The Ebro frontier revisited. In: Camps, M., Szmidt, C. (Eds.), The Mediterranean from 50,000 to 25,000 BP: Turning Points and New Directions. Oxbow Books, Oxford, pp. 293–312.
Zimmerman, D.W., 1971. Thermoluminescence dating using fine grains from pottery. Archaeometry 13, 29–52. https://doi.org/10.1111/j.1475-4754.1971.tb00028.x.